Innovations in Cardiac CTA

2

Alain Vlassenbroek, Mani Vembar,
and Michael Grass

2.1 Introduction

Coronary artery disease (CAD) is one of the leading causes of death in the western world and more than half the people who die from a cardiac event have no previous symptoms. Hence, there is a clinical need for tools that enable an early and accurate diagnosis of CAD. Cardiac computed tomography (CT) angiography provides a comprehensive anatomic evaluation of the heart. Cardiac anatomy and function, coronary plaque, and coronary stenoses can be assessed in a single study that is acquired within a short breath hold over a few heart beats.

The 4-slice CT scanners started an unprecedented technological evolution in 1998 but it is only with the advent of the 64-slice CT systems in 2004 that the realm of noninvasive coronary imaging became an integrative part of the clinical routine. Although image quality and robustness had significantly improved compared to the early days, several challenges still remained, such as radiation dose and limited low contrast resolution, motion artifacts, and the evaluation of coronary segments with severe calcifications or coronary stents. Today, reduction of radiation exposure is still at the forefront of the developments. With the introduction of large coverage multi-slice CT scanners, prospectively ECG-triggered step-and-shoot acquisition has become a robust scanning mode, with effective doses ranging from 2.7 to 4.5 mSv [1]. Further significant dose reductions have been achieved recently with the introduction of advanced iterative reconstruction techniques enabling effective patient doses going below 1.0 mSv with improvements in spatial and contrast resolutions [2]. With an increased spatial resolution, the evaluation of calcified plaques and stents can be significantly improved due to the reduced blooming artifacts. An improved low contrast enables a better intra-plaque attenuation assessment and may help to better identify the plaques with the highest risk to rupture. In addition, new developments have recently taken place in the field of cardiac CT image reconstructions to improve the temporal resolution and the image quality. Motion compensated cardiac reconstruction incorporates the knowledge of the calculated motion vector field within the iterative reconstruction process to reduce the motion artifacts [3–5].

A. Vlassenbroek, PhD (✉)
Department of CT Clinical Science,
Philips Healthcare, 80 Rue des Deux Gares,
1070 Brussels, Belgium
e-mail: alain.vlassenbroek@philips.com

M. Vembar, MS
Department of CT Clinical Science, Philips Healthcare,
595 Miner Road, Cleveland, OH 44143, USA
e-mail: mani.vembar@philips.com

M. Grass, Ph.D
Philips Research, Röntgenstraße 24-26,
22335 Hamburg, Germany
e-mail: michael.grass@philips.com

C. Smuclovisky (ed.), *Coronary Artery CTA*, https://doi.org/10.1007/978-3-319-66988-5_2

With all these significant improvements in CT technology over the past 17 years, cardiac computed tomography angiography (cardiac CTA) has become the preferred noninvasive modality for the detection and rule-out of coronary artery disease (CAD), with various multicenter studies demonstrating robust diagnostic accuracy and negative predictive value (NPV) [6–8]. However, the hemodynamic significance of CAD is unknown [9]. New advanced computational developments including flow simulations and noninvasive fractional flow reserve (FFR-CT) assessment have recently been introduced and are currently evaluated in clinical studies. The promising results, combined with the new developments in first-pass and dynamic CT myocardial perfusion imaging indicate that multi-slice CT (MSCT) has a great potential to provide comprehensive information regarding the hemodynamic relevance of coronary artery stenosis. Finally, further improvements in myocardial perfusion, delayed enhancement imaging, and vulnerable plaque detection might be anticipated with the new spectral MSCT detectors enabling dual-energy imaging.

Experimental CT designs and applications which were proposed a few years ago are now part of the current clinical reality. So we can anticipate that the current innovations in cardiac CT could facilitate early, and comprehensive diagnosis of cardiovascular disease in the near future.

2.2 Cardiac CT: Requirements and CT Technology

Noninvasive cardiac imaging is an extremely demanding field and presents a number of clinical challenges. The most critical and challenging requirement for successful cardiac CT imaging is the minimization of motion artifacts because the coronary arteries undergo complex 3D motion during the cardiac cycle. These arteries are extremely small, with diameters ranging from 5 mm in the proximal sections to less than 1 mm distally. As a consequence, excellent spatial and temporal resolution requirements are prerequisites for CT scanners to assess the coronary arteries. In addition, they must have adequate and uniform contrast enhancement for proper visualization. As the scans are performed under a single breath-hold condition, the acquisition has to be completed in the shortest possible time to avoid any respiratory motion artifacts. Patients are exposed to radiation dose and hence dose-reduction techniques need to be employed. The large volume of image data generated also presents the user with visualization and workflow challenges. Lastly, the presence of plaques poses unique challenges. Calcified plaques often make it difficult to visualize the lumen whereas noncalcified plaques demand superior spatial and temporal resolution. Cardiac imaging is thus a demanding application for CT requiring multiparameter optimization.

In the early days, CT scanners were limited to scanning the patients in axial (or "step-and-shoot") mode with a one-dimensional detection system and with a patient translation occurring in sequential steps between the scans. A complete set of X-ray attenuation data was acquired during an X-ray tube rotation around the stationary patient, and these projections were used to reconstruct cross-sectional images of the patient anatomy. The patient table was then subsequently positioned to the next axial location and the data acquisition repeated. In this fan-beam CT configuration, axial slices of the object were sequentially acquired and reconstructed using a well-known mathematical technique (2D filtered back projection (2D-FBP)) [10] and subsequently assembled to build the volume. The introduction of spiral scanning in 1990 [11, 12] enabled continuous data acquisition with simultaneous patient translation at a constant speed. Spiral scanning provided volumetric acquisitions and enabled the reconstruction of overlapping slices leading to high-resolution imaging without the need to increase the patient dose. The time to cover a

volume of interest was minimized compared to the axial mode, reducing acquisition and examination times as well as image artifacts or misregistrations caused by the patient motion between the steps. Since then, CT scanners have been subject to tremendous technological innovations. The most important improvement was the stepwise replacement of the one-dimensional detection system, which consisted of one single row of detectors, to two-dimensional large area detectors with a detector array consisting of more than a single row of detectors. A dual-slice CT scanner with two rows of detectors (CT Twin, Elscint Haifa Israel) had already been on the market since 1992 when multi-slice CT (MSCT) scanners with four rows and 0.5 s gantry rotation times were introduced in 1998 by several manufacturers. The technological innovations brought by the 4-slice scanners subsequently paved the way for applications in cardiac imaging [13]. Simultaneous acquisition of electrocardiogram (ECG) data during spiral CT scanning enabled the development of acquisition and reconstruction techniques specific to cardiac imaging. Synchronizing the location of the peak of the QRS complex in the ECG with the projection data allowed the reconstruction and visualization of anatomy at various phases of the cardiac cycle, thus making functional imaging possible. Breath-hold times of 40 s needed to cover the cardiac anatomy, however, still posed a challenge, causing many patient groups to be excluded. To reduce the scan duration and mitigate these breath-hold limitations, the number of simultaneously acquired slices had to be increased. This meant the start of the "slice race" which became a phenomenon in the early 2000s and the use of wider detector arrays allowing for faster scanning and for a more effective use of the available X-ray flux due to the increased cone angle. The increase of the number of detector rows was not without consequence. With 2D area detectors and cone-beam geometry, a 3D volume had to be reconstructed from 2D projection data, which was referred to as "cone-beam reconstruction" [14]. It resulted in a paradigm shift from two-dimensional (2D-FBP) to volumetric reconstruction approaches (3D-FBP) which required a considerable increase in the computer power of the commercially installed scanners to reconstruct the clinical images in an acceptable time. The 3D reconstruction techniques were introduced in 2001 as the basic image reconstruction technique for the 16 detector row scanners [15–17], and further extended to cardiac reconstructions [18, 19]. One important benefit of the 3D reconstructions was their volumetric approach which provided overlapping slices leading to high-resolution imaging even in the axial step-and-shoot mode. This enabled an improved longitudinal resolution in the axial mode similar to the one achieved in spiral mode. One of the consequences of the cone-beam geometry is the need to overlap the consecutive shots in the axial step-and-shoot mode. This overlap is Field-of-View (FOV) dependent and achieved by using a table feed smaller than the X-ray beam collimation in the axial mode (overlap 20% at FOV = 25 cm). Consequently, a patient's radiation exposure could increase when the acquired FOV increases [20].

Higher temporal resolution was also considered necessary in the early 2000s and cardiac CT was the driving force for the new developments. One approach to improving temporal resolution in spiral cardiac CT scans is to combine data from consecutive cardiac cycles to be used in reconstruction thereby improving the temporal resolution [18, 19]. Improvements to temporal resolution can also be achieved with a reduction of the gantry rotation times. One major limitation which is associated with faster scanning is the required X-ray power which has to be increased inversely proportional to the decrease in rotation time to arrive at a constant mAs product and to keep the image quality at the required level. Another major limitation in speeding up the gantry rotation is due to the mechanical constraints associated with the increased centripetal acceleration $\omega^2 R$, which is proportional to the square of

the rotation frequency ω and to the radius of rotation R. The typical centripetal acceleration of a single-slice CT (SSCT) with a 1 s rotation was around 3 g (where g is the acceleration due to gravity). The current generation of MSCT acquires 256–340 slices simultaneously with an extremely fast gantry rotation of ($\geq$0.25 s) and the centripetal acceleration is around 40 g [21]. To give an order of magnitude, the effective weight of the X-ray tube (approx. 40 kg at rest) during the rotation is around 1.6 tons. Thus, mechanical design has to withstand this very fast rotation and the additional forces acting on the X-ray tube. In 2005, Siemens introduced the dual source CT (DSCT) design in order to improve the temporal resolution. DSCT combined two arrays of X-ray tube plus detectors that were arranged at a 90° angle. With this configuration, the temporal resolution was expected to be improved by a factor of 2 since only 90° of rotation was necessary to acquire the 180° of projections which were needed to reconstruct the images [22–24]. New generations of DSCT have been introduced on the market, and this dual tube design is still available today to perform cardiac imaging.

The modern MSCT scanners accommodate nearly a 1000-fold increase in speed over SSCT, enabling ultra-fast heart coverage with isotropic resolution, potentially making MSCT the modality of choice for noninvasive coronary artery imaging.

2.3 The Cardiac Motion and ECG Synchronization

2.3.1 The Cardiac Motion

The coronary arteries are subject to complex 3D motion during the cardiac cycle and the suppression of the associated motion artifacts remains the greatest challenge in imaging those vessels with MSCT. Early investigations in characterizing coronary artery motion used conventional angiography [25] where the motion of the bifurcation points between the main coronary arteries and their branches were used in modeling the left-ventricular wall motion and in demonstrating the variability of the "rest period" for different coronary arteries at various heart rates [26]. Investigations with electron beam CT showed that the left anterior descending artery (LAD) moves during each cardiac cycle at a rate of 22 mm/s on average, and that the velocity can be more than 3–4 times that value for portions of the right coronary artery (RCA) [27]. Furthermore, the total excursion of the artery during the cardiac cycle is a distance that can be multiples of its own diameter. More recent MSCT velocity measurements at various landmarks along the primary coronary arteries showed that this complex 3D motion depends not only on the specific coronary artery, but also on the location along the course of the vessel and patient heart rate [28, 29].

Motion artifacts caused by this complex 3D motion can be minimized in MSCT studies by limiting image acquisition or reconstruction to those parts of the cardiac cycle associated with the least motion.

Generally, the two phases of the cardiac cycle in which the motion of the coronary arteries is minimized are the "end-systolic rest period" during the isovolumic relaxation time (IVRT) of the myocardium and the "diastasis period" (or "mid/late-diastole") which takes place between the rapid ventricular filling and the atrial contraction. At slow heart rates (<65–70 bpm), the diastasis period is the most optimal imaging period. At faster heart rates (>70 bpm), the diastasis period shrinks, making the end-systolic period the one with the least coronary motion [30].

A consequence of this fast, large, and complex 3D motion is that a high temporal resolution at MSCT is not the only requirement to successfully image the cardiac vessels; imaging the heart during the rest period of the cardiac cycle is also a necessity and will lead to an improved visualization of the coronary arteries and of the entire cardiac anatomy in general. Thus, both image acquisition and reconstruction need to be synchronized with the ECG signal of the patient to determine when the quiescent phase occurs.

2.3.2 The Cardiac Physiological Phases and the Delay Algorithm

Different approaches have been used to determine specific cardiac phases from the ECG signal.

Those techniques use the peak of the QRS complex (The *R* wave) as a reference time point in the cardiac cycle. Typical ECG-based gating techniques use either a fixed absolute delay (i.e., delay offset) or a fixed percentage delay to identify when the heart is in a given state during the cardiac cycle. The fixed absolute delay refers to the point in time (in ms) either after the arrival of the current *R* wave or before the following *R* wave where the reconstruction is performed. The percentage delay refers to the percentage of the *R*-*R* interval where the image is reconstructed. However, it is well known that the relationship between the cardiac phase and the time from the *R* wave varies nonlinearly with the heart rate. Additionally, at a slow heart rate, systole occupies roughly 1/3 of the cycle and diastole 2/3. As heart rate increases, systole increases and diastole decreases to roughly 50% each of the heart cycle. Thus, the reconstruction phase (either as a fixed or percentage delay) that is optimal at one heart rate may contain motion artifacts at a different heart rate, even in the same patient. Consequently, using a fixed delay (absolute or percentage) is not sufficient to allow for these nonlinear variations as this approach is not adaptive enough to locate the same desired phase on a consistent basis. A dynamic model using certain compliance parameters to account for the nonproportional changes, while providing an estimate of the state of the heart irrespective of the variations of the heart rate for a given patient, was proposed as an alternative [31, 32]. This model assumes that for a reference heart rate, e.g., 72 bpm, the various phases of the heart cycle are known. At this reference, end diastole is identified at 0% of the R-R cycle, end-systole between 35 and 45% and mid-diastole between 70 and 80%. As the instantaneous heart rate varies from this reference, the model adjusts the delay such that the same physiological phase can be identified and reconstructed. The model uses a combination of percentage delay and delay offset components, while also incorporating various parameters like the instantaneous heart rate, compliance parameters, and trigger latency. The compliance parameters account for nonproportional change of the various phases of the cardiac cycle with the variation of heart rate and thus enable us to capture the effects of the heart rate change on the duration of systole and diastole. This dynamic delay algorithm enables to track a desired physiological cardiac phase for a particular individual. It is modeled to adapt to the nonuniform changes in the various phases of the cardiac cycle (systole vs. diastole) for a particular patient as the heart rate changes dynamically during an acquisition (i.e., intra-patient variations). However, this model does not address the inter-patient variations. The systolic duration, while less sensitive to the variations in the heart rate for a particular individual, cannot be assumed to be the same for all patients. Two ECG synchronization techniques are commonly employed in cardiac CT: prospectively ECG-triggered axial scans and retrospectively ECG-gated spiral scans.

Finding the cardiac phase during which the heart is quasi-stationary to obtain the outmost image quality is challenging due to interpatient variability. ECG information does not always represent the heart motion with adequate accuracy. A simple and efficient technique has been introduced which is able to deliver stable cardiac phases in an automatic and patient-specific way. From low-resolution four-dimensional data sets, the most stable phases are derived by calculating the object similarity between subsequent phases in the cardiac cycle. This information is used to perform optimized high-resolution reconstructions at phases of little motion [33, 34].

2.4 Prospective and Retrospective Cardiac Synchronizations

2.4.1 Prospective Synchronization: The Step-and-Shoot Acquisition

The prospective approach is essentially the same as that used in electron beam CT (EBCT) [35]. Axial scans are initiated via triggers derived prospectively from the ECG signal of the patient using a delay subsequent to the arrival of the R peak [32]. As described in Sect. 1.2.2, this delay is typically calculated to reflect the quiescent diastasis phase of the cardiac cycle and is measured on the base of the average duration of the previous cardiac cycles. A partial-angle scan is performed, with the patient couch stationary. Upon completion of data acquisition, the couch is indexed to the next position, and the scan is initiated again via the trigger from the next R wave of the ECG signal, and so on (see Fig. 2.1a). For image reconstruction, a minimum of half a rotation of the X-ray tube is necessary, plus the fan angle (the angle subtended in the transaxial plane by the divergent X-ray beam emanating from the focal spot of the tube), thus resulting in approximately 240° partial-angle scans. The temporal resolution of this mode of scanning is thus limited by the rotation time.

In the early days of cardiac CT, the 4-slice scanner had a limited temporal resolution due to the slow rotation time of 0.5 s. This temporal resolution was calculated to be $0.5 \times (240/360) = 333$ ms. A cardiac scan with full myocardial coverage was typically acquired in 20–25 s with a limited longitudinal resolution of 2.5–3 mm obtained with nonoverlapping slices reconstructed with a 2D-FBP algorithm. The detector coverage used for this examination was 4×0.25 cm = 1 cm and the cardiac examination required an average of 15 shots. The step-and-shoot technique, with this poor longitudinal resolution, was thus not suitable for coronary artery assessment and was limited to coronary artery calcium scoring. In modern MSCT scanners, however, the increased coverage of the detection systems (8–16 cm), the faster gantry rotations ($\geq$0.25 s) and the 3D-FBP have partly removed these limitations and the step-and-shoot mode has become the preferred mode of acquisition to assess the coronary arteries during diastasis for patients having a stable heart rate $\leq$ 65–70 bpm. Complete cardiac coverage can be obtained with 2 shots of a 256-slice scanner rotating in 0.27 s, providing submillimeter overlapping slices with a temporal resolution of 180 ms.

Fig. 2.1 Illustration of prospectively ECG-triggered axial scanning (**a**) and retrospectively ECG-gated spiral scanning (**b**). (**a**) Scans are triggered with a preprogrammed delay after the arrival of the R peak. The temporal resolution t_{res} is half the scan rotation time (plus the fan angle). In case of high heart rates (short t_{RR}) and as a result of the latency in advancing the table after an axial scan, scans can be acquired at every other cardiac cycle. We note the overlap between the successive slabs which is required to perform the 3D-cone beam reconstructions. (**b**) Continuous scanning with simultaneous table feed with a low pitch factor to ensure sufficient overlap in the continuously acquired projection data to facilitate image reconstructions at multiple cardiac phases at the same longitudinal location. The locations of the individual R peaks are stored with the projection data, allowing the user to retrospectively reconstruct stacks of overlapping images in any physiological phase within the cardiac cycle. Standard temporal resolution corresponding to half the scan rotation time is achieved, but can be improved by combining projection data from multiple cardiac cycles

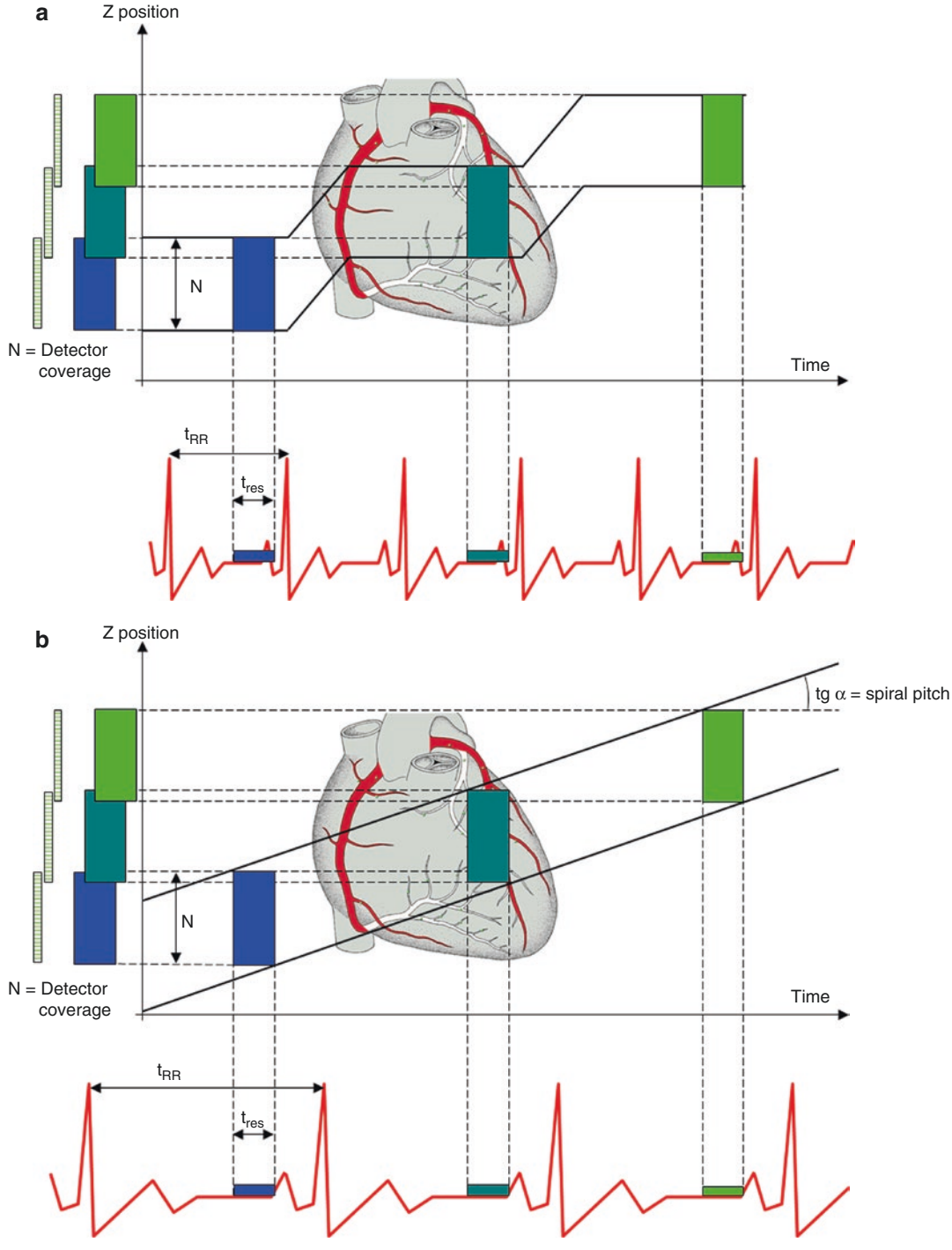
a
Z position
N
N = Detector coverage
Time
t_{RR}
t_{res}
b
Z position
tg α = spiral pitch
N
N = Detector coverage
Time
t_{RR}
t_{res}

"Phase tolerance" has been added as an acquisition option, allowing a larger scan time interval enabling the reconstruction of multiple cardiac phases centered around the targeted quiet phase with differences up to 5%. In other words, when the phase tolerance is turned ON, the step-and-shoot projection data centered in diastasis (75%) enables the reconstruction of any "mid-diastolic" phase between 70 and 80%. Of course, this increase in the duration of the X-ray irradiation is accompanied with a corresponding increase in radiation dose if the same tube current is used.

One of the limitations of prospective ECG gating is loss of image quality as a result of changes in heart rate or arrhythmia. Because each cycle of the study is an independent axial acquisition, demarcation lines are often visible between the individual steps and may be associated with step artifacts in the coronary arteries. The overlap between adjacent slabs, which is required by the 3D-FBP reconstructions, can be used to perform spatial interpolations in order to "mask" these demarcation lines and make some of the stair-step artifacts less conspicuous.

When an *R* wave arrives earlier than expected, the scan at that particular location may be acquired during a non-optimal cardiac phase resulting in blurring due to motion [36]. The likelihood of artifacts related to arrhythmia is proportional to the number of individual shots needed for the cardiac acquisition and is therefore inversely related to the detector coverage. Algorithms have been incorporated to overcome this limitation by recognizing ectopic beats in real time and to pause and wait until the next normal *R* wave is detected to continue the axial scans. In the setting of sustained arrhythmia, however, these techniques remain inferior to retrospective ECG gating.

2.4.2 Retrospective Gating: The Spiral Acquisition

For coronary CT angiography applications, spiral scanning equally provides excellent z-axis resolution with fast acquisition and volume coverage. The ECG signal is acquired simultaneously with the projection data. As the location of the *R* peak is known, the instantaneous heart rate during the scan is available. This enables the user to retrospectively reconstruct and visualize the anatomy in multiple physiological phases of the cardiac cycle, making functional imaging possible. For visualizing coronary arteries, submillimeter detector widths (ranging from 0.5 to 0.625 mm) coupled with low pitch factors (i.e., the ratio of the table feed per gantry rotation and the collimated slice width used) of 0.1–0.3 are commonly used. These low pitch factors ensure sufficient overlap in the continuously acquired projection data to facilitate image reconstructions at multiple cardiac phases at the same longitudinal location, while accounting for the variation of the instantaneous heart rate during the acquisition (see Fig. 2.1b). The continuous acquisition enables reconstruction of overlapping images with excellent longitudinal (z-axis) spatial resolution. In spiral scanning, improvement in temporal resolution is possible by combining data from consecutive cardiac cycles. This approach is useful especially at higher heart rates [37] where the diastasis is significantly reduced and the isovolumic relaxation time at the end of systole may have to be targeted for motion-free imaging. Dedicated cardiac adaptive multicycle (or multisegment) 3D cone-beam reconstruction techniques have been developed [38–40] that provide a significant improvement in the temporal resolution by combining data from as many as four cycles (see Fig. 2.2a, b). Figure 2.2c illustrates the influence of the pitch and the heart rate on the temporal resolution if a constant heart rate is assumed with the adaptive multicycle reconstruction. For each heart rate, an optimum pitch can be derived and vice versa to obtain the best compromise between the temporal resolution, the spatial resolution, and the scan duration and, hence, the given dose. If the heart rate is a harmonic or subharmonic of the rotation time, a decreased temporal resolution is obtained. The resolution

becomes worse than half the rotation time if the gating windows must be enlarged to assure that every voxel receives sufficient projection data for the 3D reconstruction. This is relevant for very low heart rates and high pitches.

With helical scans, the anatomy may be retrospectively reconstructed from different cardiac phases to compensate for changes in cardiac rhythm. The option of ECG editing is available to correct errors in ECG triggers due to the presence ectopic beats with arrhythmic patients.

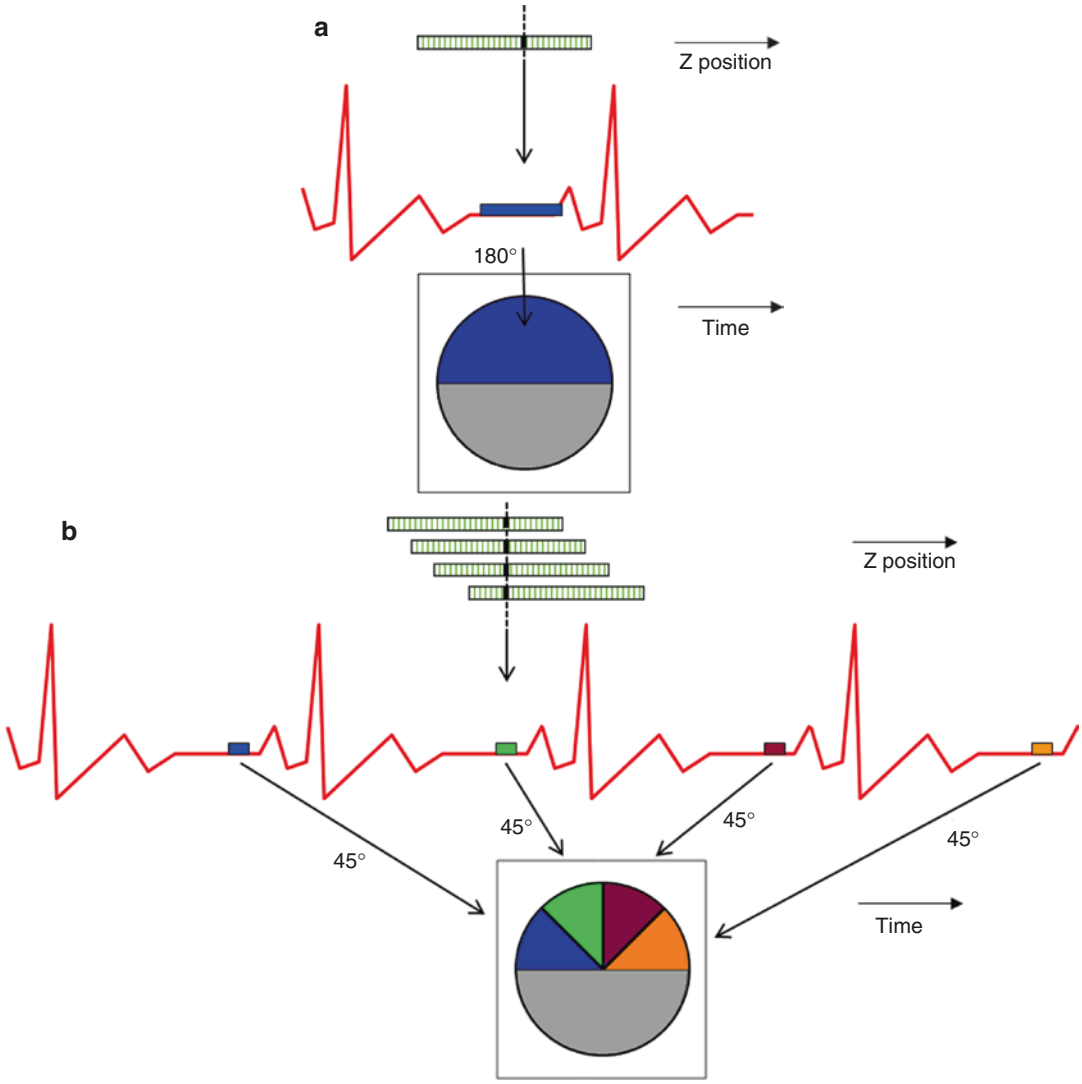

Fig. 2.2 The standard temporal resolution obtained in electrocardiogram-gated spiral scans is half the rotation time. (**a**) The circle represents the full data normally collected in one rotation of the X-ray source. Using 180°-based reconstruction approaches, the standard cardiac reconstructions obtained by information from one cardiac cycle will have a temporal resolution of 135 ms, assuming a 0.27-s rotation time. (**b**) This can be improved by combining projection data from consecutive cardiac cycles. For instance, it is possible to combine data from as many as four cycles, resulting in a temporal resolution of 34 ms, as shown here. (**c**) Illustrates the relation between the spiral pitch, heart rate, and the temporal resolution with a multicycle reconstruction. If the heart rate is equal to harmonics of the gantry rotation time, the temporal resolution is decreased. The resolution becomes worse than half the rotation time if the gating windows must be enlarged to assure that every voxel receives sufficient projection data for the 3D reconstruction. This is relevant for very low heart rates and high pitches. Note that a constant heart is assumed, without any variation

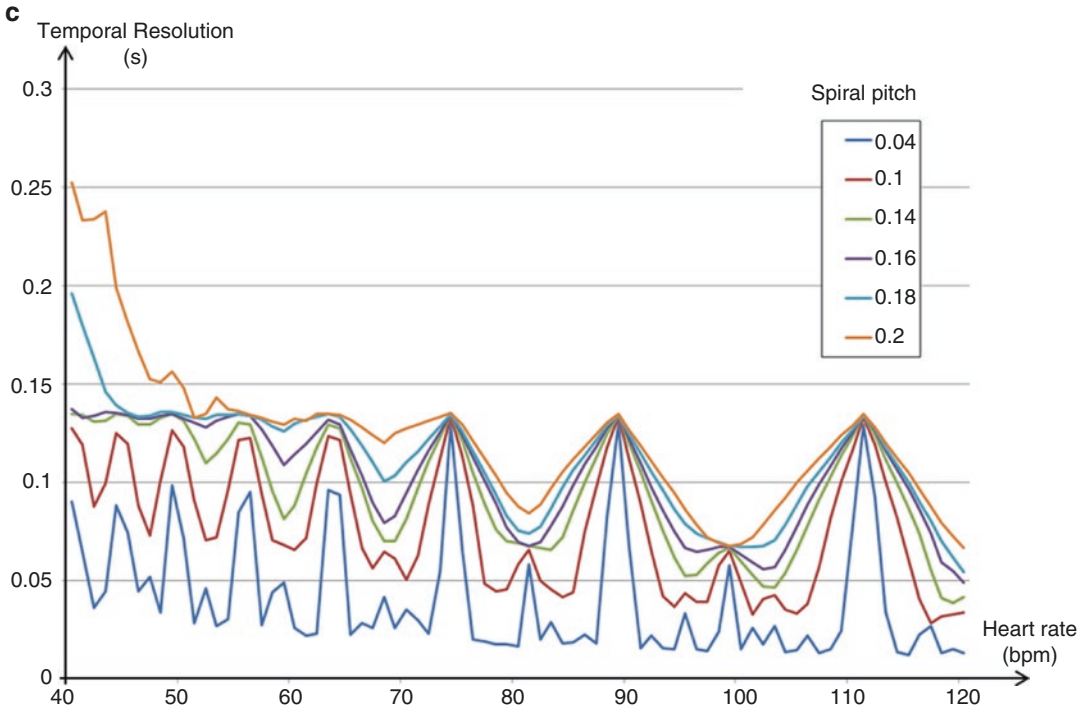

Fig. 2.2 (continued)

2.5 Radiation Exposure

2.5.1 ECG Dose Modulation

Imaging an organ over multiple physiological phases (e.g., over the cardiac cycle) can provide both anatomical and functional information (see Sect. 2.4.2). However, for many indications it is only necessary to image and expose a single phase. With the step-and-shoot cardiac techniques, the tube current is prospectively modulated to image only the desired phase in an axial scanning mode, thus enabling prospectively gated axial cardiac scanning during the "quiet" phase of the cardiac cycle. Step-and-shoot cardiac scans can result in a dose savings of up to 80% compared with a retrospectively gated helical technique [41], while maintaining optimum image quality. In other words, the roentgen tube is activated, and imaging is performed only during the short interval that is predicted to correspond to the quiet phase. In patients with a relatively regular cardiac rhythm, step-and-shoot can provide image quality and diagnostic performance equivalent to that of the retrospectively gated helical approach (see Fig. 2.3a). Coronary CTA with the step-and-shoot axial technique can image the entire coronary circulation with an average effective radiation dose from 2.7 to 4.5 mSv [1, 41].

With retrospective gating, the X-ray tube delivers radiation dose during the entire duration of the spiral scan, making it a very poor technique in terms of dose-efficiency. For this reason, ECG tube-current modulation was made available very early by all manufacturers as a dose-reduction mechanism for retrospectively gated helical coronary CTA. This technique enables to modulate the tube current during the acquisition: the tube current is kept at the nominal level (100%) during the targeted cardiac quiet phase of interest and is reduced to 20% during all other phases of the cardiac cycle, still providing sufficient image quality for the functional assessment. Using this approach, dose savings of up to 45% can be achieved without compromising the image quality in the cardiac quiet phase of interest, depending on the heart rate during

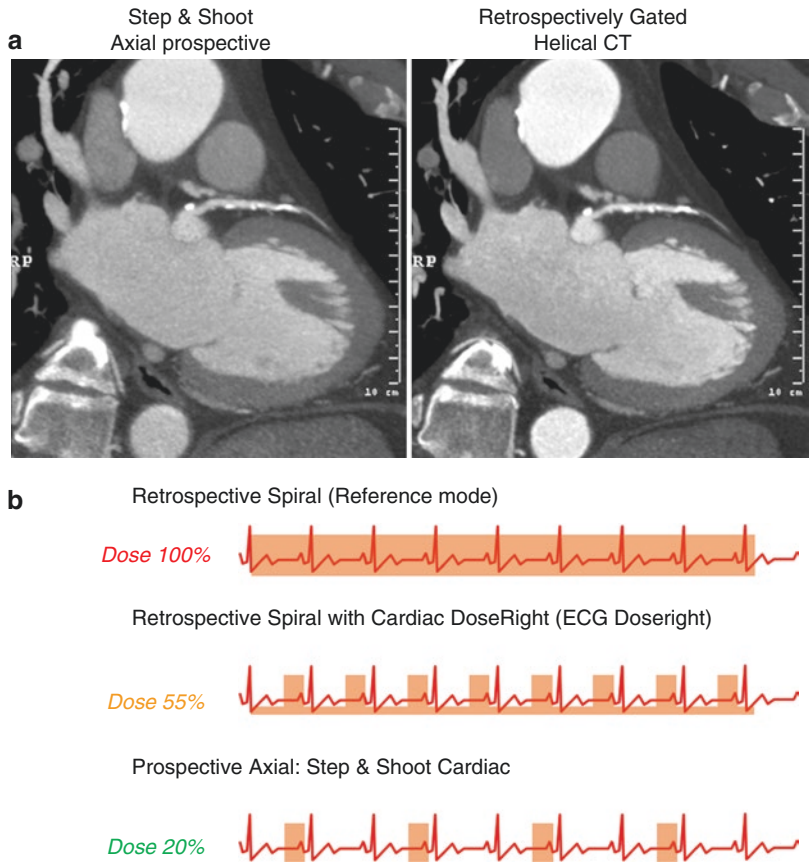

Fig. 2.3 (**a**) In patients with a relatively regular cardiac rhythm, step-and-shoot can provide image quality and diagnostic performance equivalent to that of the retrospectively gated helical approach. In this example, the full prospective axial acquisition delivered a patient dose of 2.8 mSv and the helical acquisition a dose of 11.9 mSv. (*Image courtesy of: Dr. John A. Osborne, MD, PhD, FACC, State of the Heart Cardiology, Grapevine, TX, USA*) (**b**) With retrospective gating during spiral scanning, the tube current can be kept at the nominal level (100%) during the targeted cardiac phase of interest (in this example, the diastolic phase) and can be reduced to 20% during all other phases of the cardiac cycle. Using this approach, dose savings of up to 45% can be achieved without compromising the image quality in the cardiac phase of interest, depending on the heart rate during the acquisition. With prospective gating, the tube current is prospectively modulated to image only the desired cardiac phase in an axial scanning mode. Step-and-shoot cardiac can result in a dose savings of up to 80% compared with a retrospectively gated reference helical technique

the acquisition (see Fig. 2.3b). Of course, tube-current modulation has to be prescribed prospectively which means that it suffers, to a certain extent, the same weakness as the step-and-shoot acquisition, in cases of heart rate variations or arrhythmia during the scan. In that case the peak tube current can be delivered during a wrong cardiac phase, providing noisy images during the quiet cardiac phase. Arrhythmia detection is usually available to cancel the ECG tube-current modulation for the remainder of the acquisition in case an irregular beat is detected.

2.5.2 Iterative Reconstructions

The most basic method to reduce radiation dose is to reduce the X-ray tube output. However, scans performed at lower tube currents and peak kilovoltage will have a lower signal-to-noise and projection data will appear noisy. Filtered back projection algorithms (2D-FBP and 3D-FBP) have been the industry standard for CT image reconstruction for decades [10]. While it is a very fast and fairly robust method, FBP is a suboptimal algorithm choice for poorly sampled data or for cases where noise overwhelms the projection

signal. Such situations may occur in low dose or tube-power-limited acquisitions. Noise in CT projection data is dominated by photon count statistics. As the dose is lowered, the variance in the photon count statistics increases disproportionately [42]. When these very high levels of noise are propagated through the reconstruction algorithm, the result is an image with significant artifacts and high quantum mottle noise. Over time, incremental enhancements were made to FBP to overcome some of its limitations. These improvements continued until recently, when a completely different approach to image reconstruction was explored through the clinical implementation of iterative reconstruction (IR) techniques. These algorithms differ from FBP methods in that the reconstruction becomes an optimization process that takes into account the data statistics, image statistics, and system models [43]. IR algorithms use initial estimates of the voxel attenuation to predict projection data. These estimates are then iteratively adjusted to minimize the difference between the predicted projection data and the measured projection data. The noisiest measurements are given low weight in the iterative process; therefore, they contribute very little to the final image. Hence, IR techniques treat noise properly at very low signal levels, and consequently reduce the noise and artifacts present in the resulting reconstructed image. This results in an overall improvement of image quality at any given dose. With IR techniques, the noise can be controlled for high spatial resolution reconstructions; hence providing high-quality, low contrast, and spatial resolution within the same image (see Fig. 2.4). While IR techniques have been used for many years in PET and SPECT imaging, the sampling density and the data set sizes in CT have historically caused IR techniques to perform extremely slowly when compared to FBP. However, recent innovations in hardware design and algorithm optimizations have permitted the clinical use of IR technique in CT. Recent clinical studies showed that additional dose reduction can be achieved with IR techniques in cardiac imaging [44].

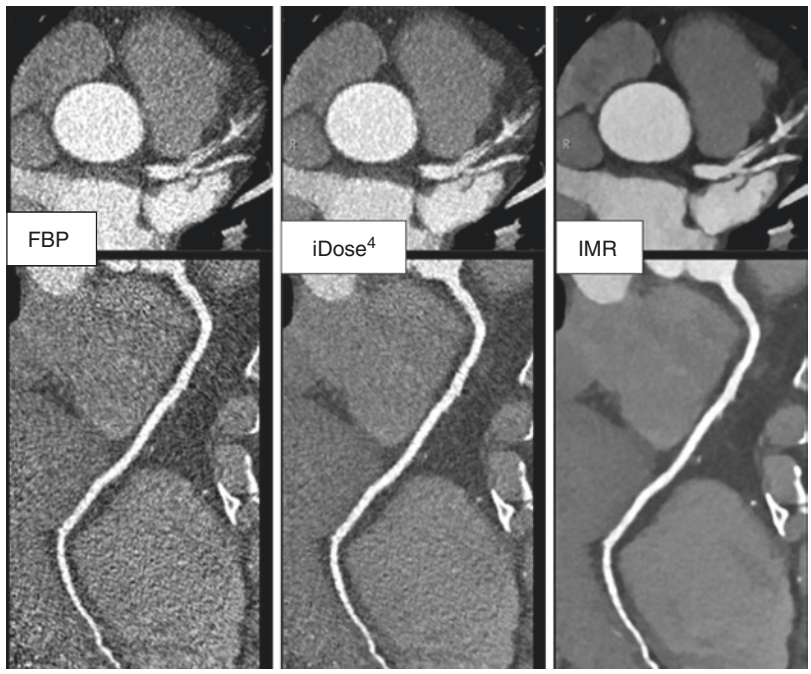

Fig. 2.4 This clinical study provides an example of the expected image quality improvement that may be achieved with two generations of iterative reconstructions (iDose^4 and IMR, Philips Healthcare, Cleveland, OH, USA). An ECG-gated coronary CT angiogram scanned with the step-and-shoot technique on a Philips iCT at 0.9 mSv (100 kVp, 110 mAs, 5.2 mGy, 67.1 mGy cm) and reconstruction with FBP (*left*), iDose^4 (*center*), and IMR (*right*). Study shows limited visualization of soft-plaque on FBP. With the latest generation of IR (IMR), there is a clear improvement in spatial resolution, low contrast, and noise characteristics (*Image courtesy of: Amakusa Medical Center, Japan*)

2.6 Image Post-processing

The amount of data produced by multidetector CT scanners as well as the time needed to review the resulting several thousand slices (e.g., 10 reconstructed cardiac phases with 400 slices each) have been continuously increasing, providing a workflow and diagnostic challenge to the clinician. Therefore, automatic image processing methods became a prerequisite to efficiently analyze the large amount of image data produced by cardiac CT during cardiac exams. Simple image-based segmentation methods like global thresholding, region growing, etc. usually fail to automatically segment an image because of noise, limited resolution, partial volume effect, or similar gray-value characteristics of different organs. With these methods, user interaction is needed to either initiate segmentation, control the progression of the algorithm, and/or to correct for segmentation errors [45, 46]. This may be time consuming and distracts the physician from his/her actual diagnosis. To overcome these limitations, sophisticated model-based methods for a reliable and automatic segmentation of the four cardiac chambers and major coronary arteries have been proposed. Shape-constrained deformable model for heart segmentation have been described in detail in [47]. These algorithms adapt an anatomical model of the heart chambers and main trunks of the coronary arteries to the MSCT image volume (see Fig. 2.5). They are coupled with automated vessel tracking algorithms, which provide curved multi-planar reformations of the individual coronary arteries, enabling automatic measurements, including that of coronary artery

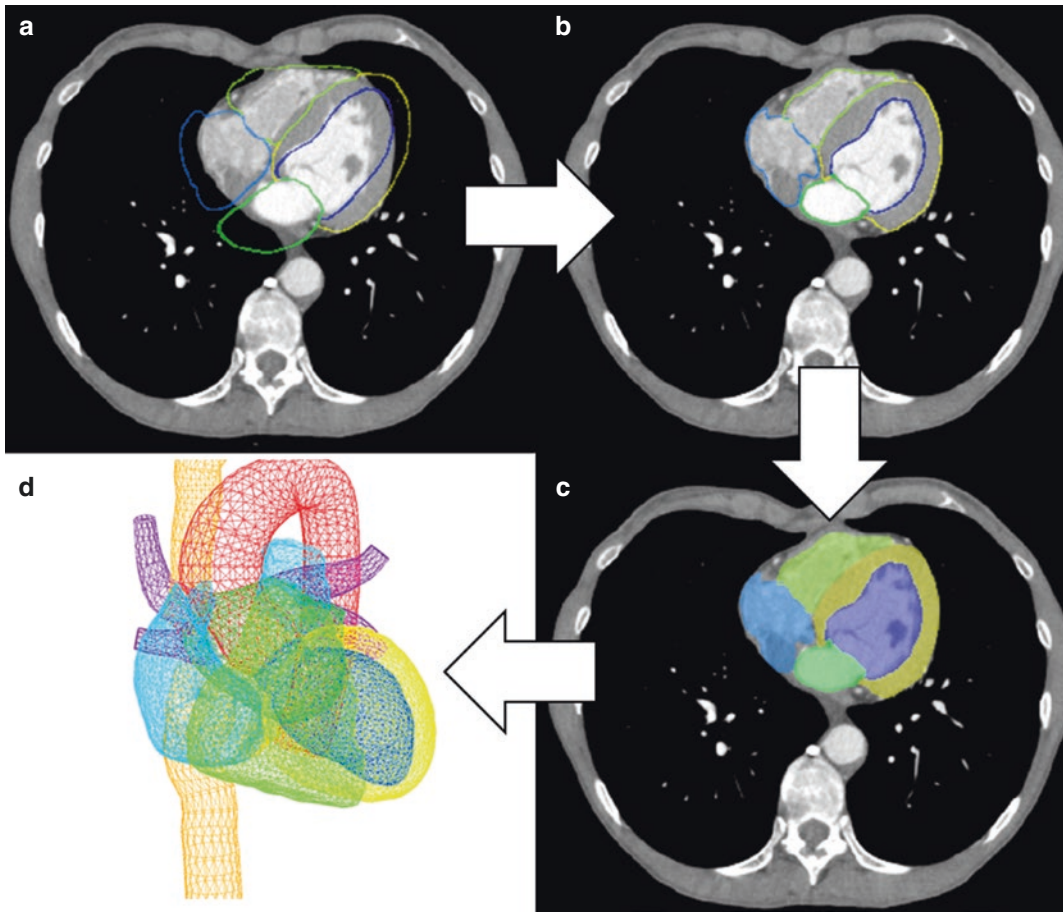

Fig. 2.5 After loading a trained cardiac model, boundaries of the heart are matched to the model, resulting in a segmentation of the various anatomic structures of the heart (a > d). A triangulated mesh model of the endocardial surfaces of the four cardiac chambers as well as the left-ventricular epicardium and short trunks of the major vasculature is obtained

area, diameters, and stenosis extent. An important application of the model-based methods is the successful automatic assessment of the global heart function in multiphasic retrospective cardiac studies [48]. The geometric heart models resulting from segmentation have been increasingly used to guide invasive therapeutic procedures. It has been proposed, for instance, to overlay heart models onto live fluoroscopy data to support ablation procedures for treating atrial fibrillation [49, 50] or stem cell injection for myocardial repair [51, 52]. For these applications, a heart model comprising only the four chambers and the main coronary arteries is often insufficient. It is, for instance, important to extract the left atrium and the proximal part of the pulmonary veins to support guidance of ablation procedures for atrial fibrillation treatment. For cardiac resynchronization therapy, a heart model including the coronary sinus is needed to facilitate implantation of the pacemaker lead.

2.7 Cardiac MSCT Future Directions

2.7.1 Myocardial Perfusion Using Cardiac CTA

Noninvasive myocardial perfusion imaging (MPI) using single-photon emission computed tomography (SPECT) has been the standard-of-care for the assessment of physiologic significance of coronary lesions, with studies showing good correlation of the infarcted and ischemic burden with long-term outcomes thereby aiding in the decision-making for medical therapy versus revascularization [53]. Magnetic resonance imaging (MRI) has also been used for the detection of myocardial regions that have a delayed wash-in of contrast which shows up as hypo-enhanced regions both under rest and pharmacological stress (indicating myocardial infarction) or only under stress (reversible defects or ischemia). In addition, MRI is also considered as the gold standard for the assessment of myocardial regions with a delayed wash-out of contrast, wherein imaging performed with a delay of 5–10 min after administration of contrast could show regions of hyper-enhancement indicating myocardial scar [54]. The presence of these delayed hyper-enhanced regions has been associated with adverse left-ventricular (LV) remodeling [55]. A combined analysis of early- and late-enhancement regions could provide additional information on the tissue viability and functional recovery after coronary revascularization [56].

The ability to provide anatomical and physiologic information could further expand the role of cardiac CT. Depending on the mode of scan performed, a comprehensive assessment of coronary arteries, myocardial perfusion defects, regional wall motion, and left-ventricular (LV) function can be obtained from a single scan. Such a comprehensive exam using CT comprises a stress scan, followed by a rest scan and in some cases a delayed scan [57–59].

A typical protocol is shown in Fig. 2.6. Patient preparation includes avoidance of caffeine for at least 12 h prior to the exam and medications such as nitroglycerine. Stress is typically induced pharmacologically (adenosine) by which blood flow is increased in the normal coronary segments and reduced in the diseased segments, causing the heart rate to elevate. The surview (scout) is used to plan the scans—typically from the carina to the diaphragm. Scans are initiated when the contrast reaches a threshold in the ascending or descending aorta (determined via a test bolus or automated bolus tracking). A volume of 50–70 cc of contrast is given at the rate of 5–6 cc/s designed to provide peak contrast enhancement in the coronary arteries.

Stress scans are typically performed using the conventional helical retrospective-gated techniques, with or without ECG-tube modulation (which could provide some radiation dose reduction). This enables multiple phases to be used for functional and perfusion assessment. The availability of multiple phases also helps to differentiate perfusion defects (which typically show up across all phases of the cardiac cycle) from artifacts (which may be seen in only one phase and may be mistaken for a perfusion defect). The selection of the tube voltage (kVp) and the current (mA) is based on the body habitus of the patient (based either on weight-based or body-mass-index [BMI]). The adenosine infusion is

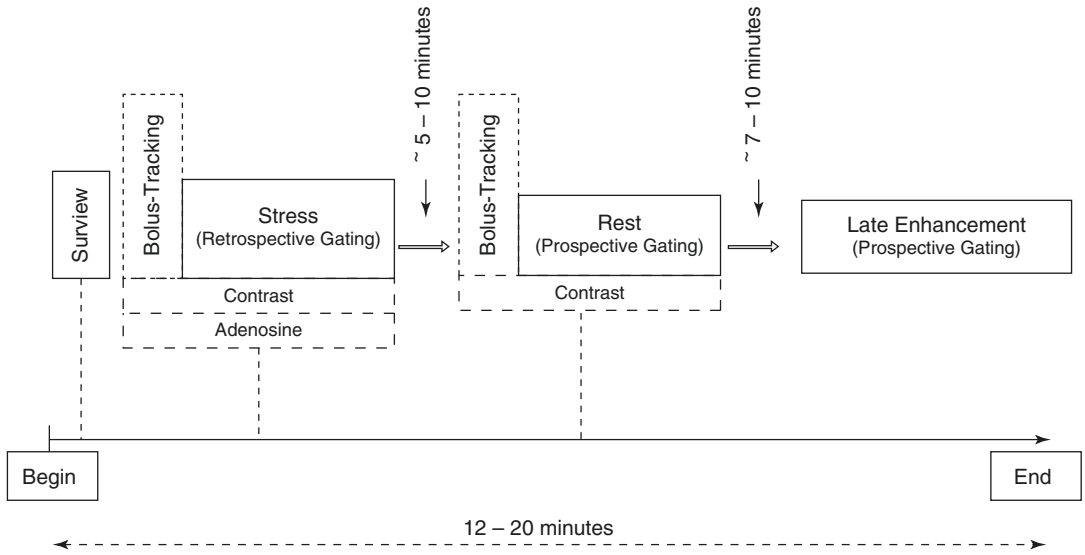

Fig. 2.6 A typical protocol for stress perfusion using CT

given at the rate of 140 μg/kg/min and stopped immediately at the conclusion of the scan.

Following the scan, the patient's vital symptoms are monitored while allowing the heart rate to return to the baseline in preparation for the rest scan. This typically takes 5–10 min. Once the heart rate is back to the baseline, beta-blockers are administered to lower and stabilize the heart rate and sublingual nitroglycerine given to dilate the arteries. For the rest scan, prospective-gated acquisition is commonly used to reduce radiation dose to the patient, with the targeted cardiac phase centered at 75% of the R-R cycle, corresponding to ventricular diastasis. For consistency, the value of kVp is kept the same as in the stress acquisition.

The third scan is a late-enhancement scan performed 7–10 min after the last contrast injection (in this case, after the rest scan). This is meant for the detection of hyper-enhanced regions (late enhancement) that could indicate myocardial necrosis [57, 58, 60]. As with the rest scan, prospective gating is used to reduce radiation dose, along with the use of a lower kVp (e.g., 100 kVp), and a thicker slice for reconstructions (e.g., 2 mm).

For the assessment of perfusion defects from all the three scans, images are usually visualized in a short-axis orientation. Images are viewed in thick slices (e.g., 5 mm) to reduce noise and improve contrast resolution. A narrow window and level setting is typically used (e.g., window of 150–200; level of 100). From the assessment of short axis images, it is possible to distinguish reversible defects (hypo-enhanced regions that show up only in stress scans) from the fixed defects (hypo-enhanced regions that are exhibited in both stress and rest scans). Figure 2.7a, b is an example of a short-axis image from a scan performed under stress exhibiting hypo-enhanced regions in the basal anteroseptal and basal inferolateral walls caused by lesions in the proximal LAD and LCX. The use of advanced iterative reconstructions, such as iterative model reconstruction (IMR) (Fig. 2.7b), could help reduce noise with improved low contrast detectability compared to filtered back projection (FBP) (Fig. 2.7a). Figure 2.8 is an example of a scan (of a different study) taken 7 min after the administration of contrast, showing late hyper-enhancement in the inferolateral wall indicating myocardial necrosis (infarct).

The sequence of the scans (stress followed by rest or vice versa) could be determined based on the risk factors. For patients with a low likelihood of disease, it may be preferable to administer beta-blockers, stabilize the heart

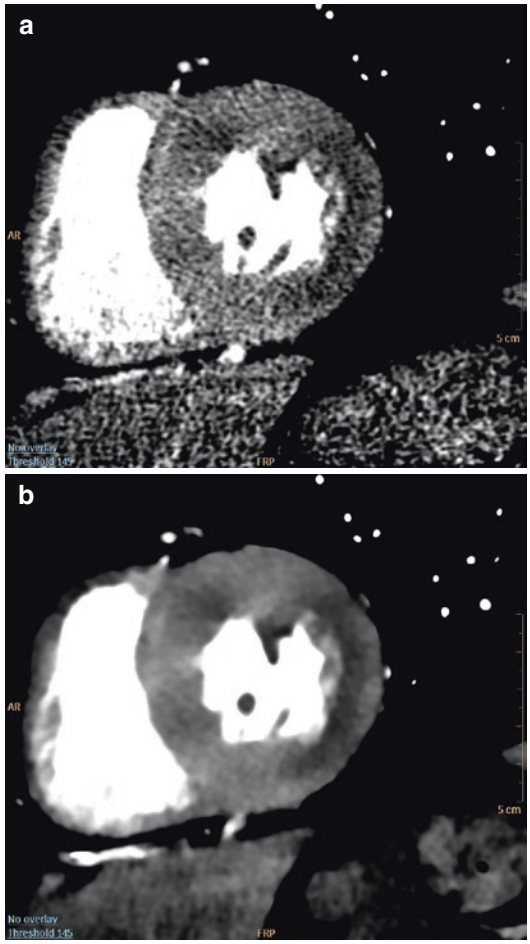

Fig. 2.7 (**a**, **b**) Is an example of a short-axis image from a scan performed under stress exhibiting hypo-enhanced subendocardial regions in the basal anteroseptal and basal inferolateral walls caused by lesions in the proximal LAD and LCX. The use of advanced iterative reconstructions, such as iterative model reconstruction (IMR) (**b**) could help reduce noise with increased low contrast detectability compared to filtered back projection (FBP) (**a**) (*Image courtesy of: Drs. G. Colin and B. Ghaye, Clinique universitaires Saint-Luc (UCL), Brussels, Belgium*)

rate, and perform a rest scan first. If no disease is found, a second scan can be avoided thereby resulting in radiation dose savings. On the other hand, since a stress scan may be more relevant in these exams especially in patients with intermediate likelihood of disease, performing this scan first may provide a more accurate assessment of the myocardium by avoiding any venous contamination from a prior injection used in a rest scan.

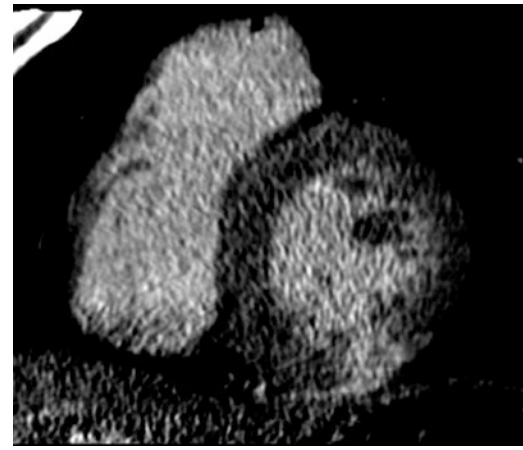

Fig. 2.8 A short-axis representation from a delayed scan performed 7 min after the injection of contrast, showing late hyper-enhancement of the mid inferolateral portion of the myocardium indicating myocardial damage (*Image courtesy of: Prof. L. Boussel, Hospices Civils de Lyon, Lyon, France*)

The perfusion assessment using cardiac CTA provides valuable adjunct information for the determination of hemodynamic significance of CAD, thus expanding the role of cardiac CTA. However, quantification (or semi-quantification) of the myocardial blood flow is still lacking since it requires a dynamic examination (again, typically performed under pharmacological stress) and the aforementioned scans are performed at a single time point. Various preclinical and clinical investigations have studied the feasibility of ECG-triggered dynamic myocardial perfusion (DMP) using CT targeting a physiologic cardiac phase for imaging over time. Dynamic scans with a narrow detector [61–63] require a back-and-forth table translation to cover the complete or a significant portion of the LV myocardium. Due to the lack of coverage, the superior and inferior sections of the myocardium are imaged at different time points which could require the user to employ a different arterial input function (AIF) for each "slab." Additionally, these scans are ECG-triggered and typically performed at higher heart rates (75–90 bpm), resulting in a lower temporal sampling at a given location which could impact quantification of perfusion measurements. Wide area detectors remove the need for table movement, allowing the user to program the sampling

interval accordingly (i.e., optimize the radiation dose) while at the same time providing imaging of a more homogenous distribution of contrast across the entire LV myocardium [64–68]. The quantification of perfusion is further improved with the use of elastic registration and temporal filtering to reduce anatomical motion and the presence of any noise spikes [67, 69]. Prior to the dynamic scans, the time corresponding to the peak contrast enhancement in the LV is first determined via a series of time lapse scans; alternatively, it can also be derived from a coronary CTA scan if such a scan is performed first as part of the overall cardiac exam. Once this is known, ECG-triggered dynamic scans can be initiated 5–6 s prior to the peak enhancement in order to establish a series of baseline measurements. By imaging over time and thus capturing the instance of the peak enhancement of the left ventricle, any reduction (or slow uptake) of blood flow in the regions of myocardium (ischemic regions) corresponding to the culprit coronary artery can be imaged and quantified. Figure 2.9 is a short-axis color-map representation from a DMP CT scan of a patient showing reduced peak enhancement in the inter-ventricular septum (blue regions) corresponding to a lesion in the mid-LAD.

One of the main drawbacks of the DMP-CT scans is the radiation dose. While reduction of tube energy and/or current is one obvious approach to address this, it can be complemented with the use of other innovative techniques. By adjusting the temporal sampling or with the use of appropriate levels of advanced reconstruction techniques (such as iterative approaches), further reductions in radiation dose reductions can be achieved, as demonstrated in early preclinical investigations [64, 70, 71].

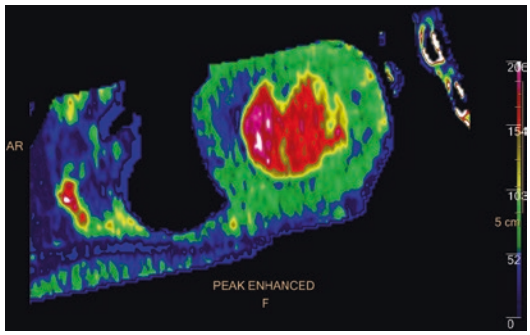

Fig. 2.9 A color-map representation of a short-axis image from a dynamic myocardial perfusion CT scan showing regions with low enhancement in the inter-ventricular septum (in *blue*) caused by a lesion in the mid-LAD (*Image courtesy of: Drs. Armin Huber, Daniela Muenzel and Bettina Gramer, Klinikum rechts der Isar der Technischen,Universität München, Munich, Germany*)

2.7.2 Fractional Flow Reserve Using CT (FFR-CT)

A newer alternative approach using cardiac CTA to determine the hemodynamic significance of a coronary lesion is gaining interest. Traditionally, the concept of fractional flow reserve (FFR), which represents the ratio of pressure distal to a lesion compared to the portion of the artery proximal to the lesion (i.e., "normal" section, or aorta) is the most commonly accepted approach for the assessment of lesion-specific ischemia—a value of ≤ 0.8 is considered hemodynamically significant. However, FFR is measured in the cath labs, as part of an invasive procedure. Recent work has focused on extending the role of cardiac CTA beyond anatomy for improved clinical decision-making.

Novel approaches (FFR-CT) are being developed that use the existing cardiac CTA data to simulate a drop in pressure in the presence of a coronary lesion [72–74]. These approaches are computationally intensive but have shown promise and good correlation with the gold standard (invasive FFR), making it possible to have a single non-invasive imaging test that can provide anatomical information along with physiology. This capability to include physiologic information to anatomy could make it possible to identify patients appropriate for coronary revascularization.

2.7.3 Motion Analysis and Compensation in Cardiac CT

The motion of the heart is one of the major challenges in cardiac CTA. Diagnostic accuracy is decreased when motion artifacts occur

in reconstructed tomographic images [75]. At the same time, knowledge about the cardiac motion pattern is an additional source of clinically useful information including, e.g., wall motion, ejection fraction, or valve motion [76, 77]. Novel approaches have been developed to address both challenges, functional motion analysis and motion artifact reduction, for improved anatomic analysis.

There are different approaches to detect and calculate motion in cardiac CT data sets. These include motion tracking and estimation from projection or image sequences [4, 78] or combined reconstruction of the image data and the motion vector field [79]. While the first approaches basically rely on image processing techniques like model-based segmentation (see Sect. 2.6) of image registration, the latter ones combine image reconstruction and optimization methods. All methods have in common that they finally aim to deliver a dense sampled 3D motion vector field [80] describing the temporal shape change of the anatomy for the time covered by the image or projection sequence. Figure 2.10 shows a surface representation of a heart segmented from a multi-phase cardiac CTA data set with a motion vector field at a single time point during the cardiac cycle displayed as arrows on the cardiac surfaces. The direction and length of the arrow represent the motion direction and strength. The data have been derived from a patient data set using model-based segmentation (see [81] for more details).

With this information available, functional information of the heart like the motion pattern of a coronary artery or the myocardium, temporal changes of the chamber volume, wall motion abnormalities, or even the motion of the cardiac valves can be derived. Using modern image processing techniques, the motion vector field can be analyzed qualitatively and quantitatively for selected cardiac structures.

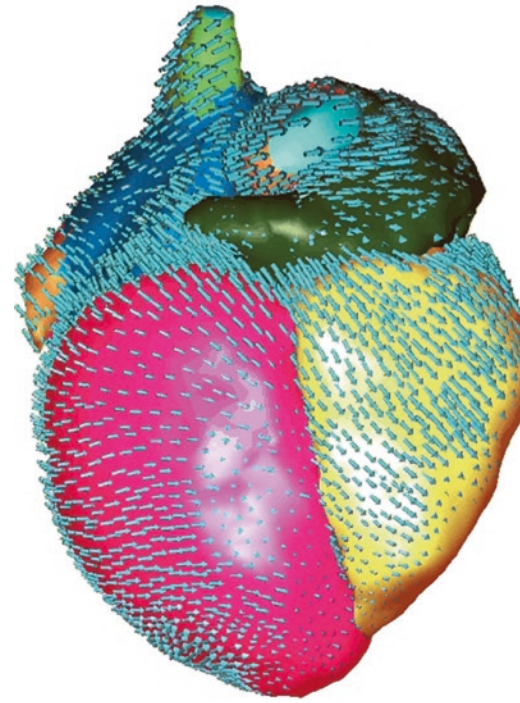

Fig. 2.10 A surface representation of a heart segmented from a multi-phase cardiac CTA data set with a motion vector field at a single time point during the cardiac cycle (displayed as arrows on the cardiac surfaces). The direction and length of the arrow represent the motion direction and strength

In addition, the calculated dense motion vector fields can be used subsequently in a motion compensated cardiac reconstruction method. Here, the filtered back projection [81–83] or iterative reconstruction [3, 4] scheme incorporate the motion vector field and thus deliver images with improved temporal resolution and image quality. The increase in image quality and definition of the cardiac anatomy will improve image-based diagnosis (see Fig. 2.11), while at the same time supplementing more sophisticated approaches involving advanced image analysis like myocardial perfusion and FFR described earlier.

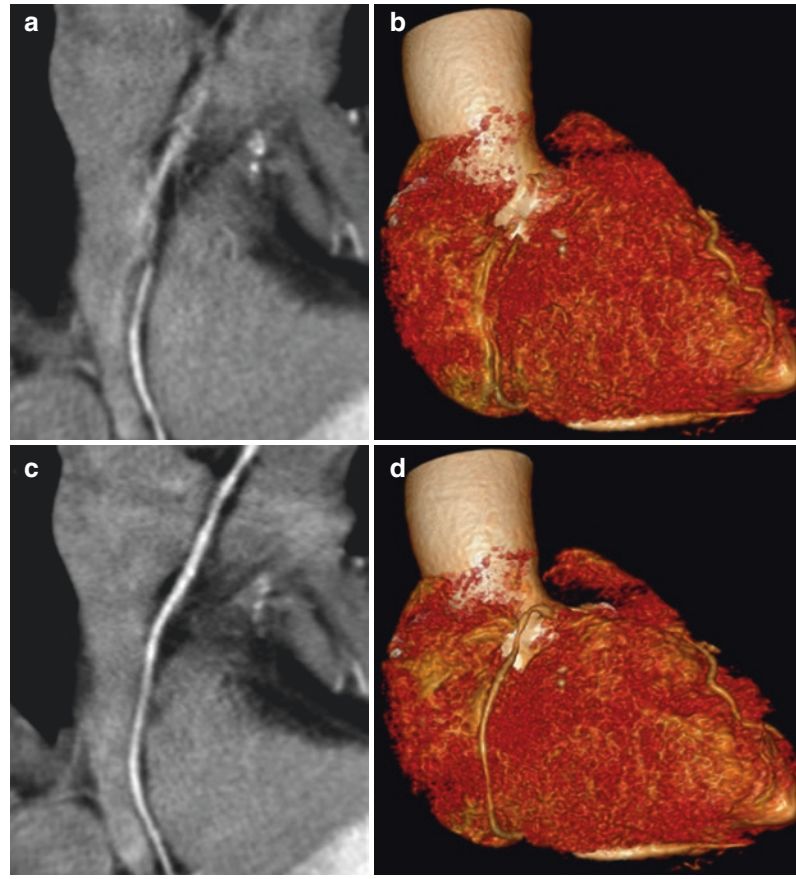

Fig. 2.11 Retrospectively gated helical cardiac reconstruction without (**a**, **b**) and with (**c**, **d**) motion compensation using the same amount of projection data during the filtered back projection reconstruction. Curved MPR (left column; L/W: 200/500 HU) of the right coronary artery and volume rendering (right column) of a patient data set with a mean heart rate of 82 bpm. The reduced motion artefact level can be clearly observed

2.7.4 Cardiac Spectral MSCT

Recent developments in scanner and detector technology and modern clinical requirements, like quantitative computed tomography and the need for tissue classification, have revived interest in spectral computed tomography. The current clinical spectral CT scanners enable the discrimination between different materials based on the differential X-ray attenuation properties in two "energy bands" of the spectrum instead of averaging the entire polychromatic beam like conventional CT does. In other words, the spectral dependencies of the net X-ray attenuation can be imaged and analyzed as a material characteristic and can be used to discriminate materials. With Dual Energy CT (DECT), this additional information can be obtained using several data acquisition methods: (1) Single X-ray source, Dual kVp Spin (Philips), (2) Single X-ray source, Dual kVp Switch (General Electric), (3) Dual X-ray source (Siemens), and (4) Single X-ray source, Dual-Layer Detector (Philips) [84, 85].

In a single source, dual-layer detector scanner configuration, one X-ray tube is used to expose a detector consisting of two layers of scintillators (Fig. 2.12). The two layers are directly on top of one another. A single CT scan is performed at a high kVp (e.g., 120 or 140 kVp). The first layer encountered by the X-ray photons absorbs most

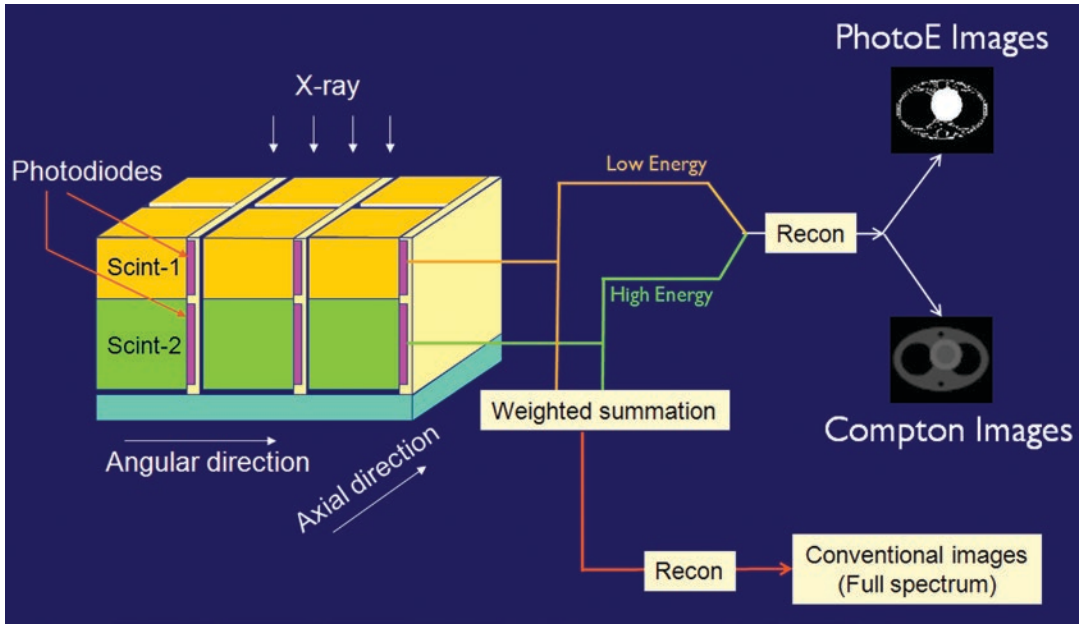

Fig. 2.12 A schematic illustration of the dual-layer detection system (only a few detector elements are shown). The photodiodes are parallel to the X-ray direction, attached to the sides of the two types of scintillator elements

of the low-energy spectrum, while the bottom detector layer absorbs the remaining higher energy photons. In contrast to other approaches of dual-energy CT, there is no need to redundantly expose materials with both low and high-energy X-rays. Furthermore, since the spectral energy separation is intrinsic to the detection system, rather than sequentially generated at the X-ray source, this approach eliminates the time lag of sequential techniques, making it ideal for imaging moving organs, as in the case of cardiovascular imaging. In other words, the dual-layer technique is fully registered both spatially and temporally. It has no spatial shift or dead time such as in dual kVp or dual tube techniques and this allows for projection space-based decomposition, and thus the opportunity for accurate beam hardening correction without the need for spatial or temporal interpolations (Fig. 2.13) [86, 87]. The low- and high-energy spectral attenuations can also be easily combined and used to reconstruct a conventional CT image reflecting the "full spectrum" attenuation without the need to compensate for warping and shifting due to the time lags. The use of a single source also obviates the cross scatter limitation of dual source techniques [88]. Furthermore, this approach allows full 50 cm Field-of-View (FOV) imaging so it can be used for both fast and large FOV MSCT cardiac spectral imaging, without any compromise.

The first investigations of dual energy methods for CT were made by Alvarez and Macovski in 1976 [89]. They demonstrated that, using a conventional X-ray source having a broad energy spectrum, one can separate the X-ray attenuation coefficients into the contributions from the photoelectric effect and Compton scatter. In other words, Alvarez and Macovski demonstrated that the X-ray attenuation coefficients of common materials can be expressed with sufficient accuracy as a linear combination of the photoelectric and Compton attenuation coefficients. As a consequence, the X-ray attenuation coefficients of any material can be expressed as a linear combination of the attenuation of two basis materials, where both materials differ in their photoelectric and Compton characteristics. If bone and water are chosen as the basis material for example, the information from the low and high attenuation data can be used to calculate the bone coefficients of the X-ray attenuation. These coefficients can

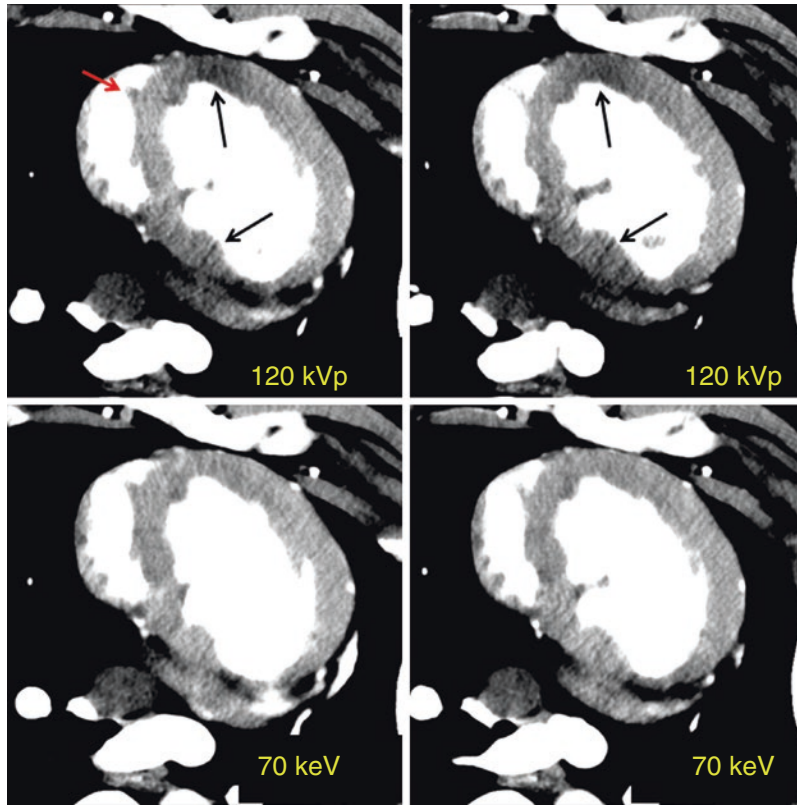

Fig. 2.13 Two different axial cardiac slices of a pig heart, corresponding to the conventional 120 kVp and the 70 keV monoE, respectively, under the condition FFR = 1. In this case, one should expect a relatively uniform enhancement on the nonischemic myocardium. However, due to BH artifacts, clear hypo-enhancements are noticed in the anterior and inferior walls in the conventional images as indicated by the black arrows. These artifacts can be misdiagnosed as perfusion defects. Hyper-enhancement in the septal wall (*red arrow*) is also the result of BH effects. On the other hand, these BH-induced hyper- and hypo-attenuations are significantly reduced on the 70 keV images resulting in a relatively more uniform enhancement of the entire myocardium (*Image courtesy of: Drs. Rachid Fahmi & David Wilson, Case Western Reserve University, Cleveland OH, USA and Dr. Hiram Bezerra, Harrington Heart & Vascular Center, University Hospitals Case Medical Center, Cleveland, OH, USA*)

then be used to create a bone image, which allows the assessment of bony structures and calcifications. Alternatively, the water coefficients can be calculated to generate a soft tissue image where the bony structures are suppressed and which improves the visualization of structures previously hidden by bony anatomy. Other pairs of basis material with clinical relevance are iodine and calcium or iodine and water. In cardiovascular imaging, the iodine images obtained from an iodine-calcium decomposition can be of primary importance because they can help to better assess the iodinated lumen of the coronary arteries which could be otherwise hidden by the presence of large calcified plaques. The water images obtained from an iodine-water decomposition is one in which all of the iodine is removed. This virtual non-contrast image (VNC) synthesizes a pre-contrast scan.

The photoelectric coefficient depends strongly on the effective atomic number Z (photoelectric effect proportional to Z^3) and thus provides an indication of the composition of the object. The Compton scatter coefficient depends on the electron density, which is proportional to the mass density for most materials. So the use of the information obtained by the decomposition of the X-ray attenuation coefficients of any material

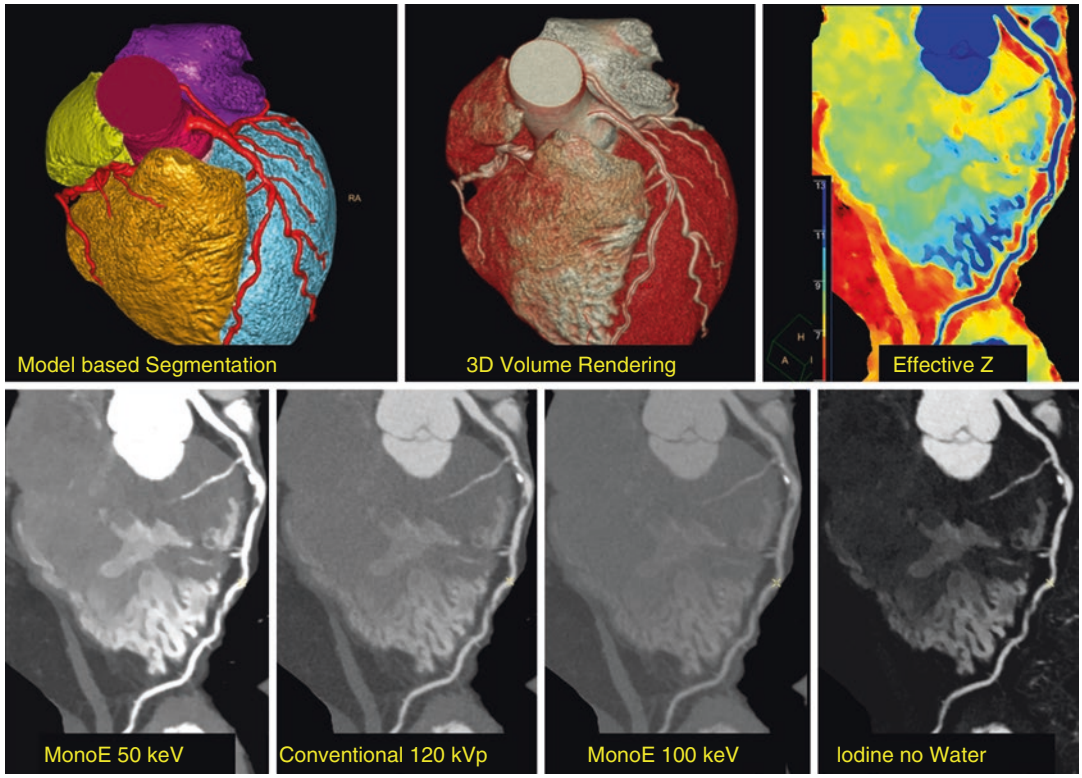

Fig. 2.14 Dual Energy measurements enable the generation of material-specific images like the effective Z images or the iodine images obtained after iodine-water decomposition. In addition, virtual monochromatic images at different energies can be synthesized and used for routine diagnosis similar to conventional images (obtained at 120 kVp in this example). Low keV (50 keV shown here) can be used to enhance the photoelectric absorption of high effective Z materials like iodine. High keV (100 keV) can be used to maximize the Compton scatter and hence minimize all types of artifacts (calcium blooming, etc.) (*Image courtesy of: Dr. Kazuhiro Katahira, Kumamoto Chuo Hospital, Kumamoto, Japan*)

into its photoelectric and Compton attenuation coefficients can be highly significant for medical purposes. For example, a lesion of increased attenuation coefficient can be due to either increased density or increased effective atomic number due to calcification. A dual-energy measurement can distinguish between these phenomena, and a color mapping of the effective atomic number Z provides a visual assessment of this additional information as is demonstrated in Fig. 2.14 [90]. In dual-energy CT, besides the material-specific information and images, one may also synthesize monochromatic images at different energies [91], which can be used for routine diagnosis similar to conventional images. With a single scan at usual 120 kVp (or 140 kVp for obese patients), a dual-layer spectral CT acquisition allows the reconstruction of virtual monochromatic images from 40 keV up to 200 keV. Since the photoelectric effect is dominant at lower keV and is relatively high for high Z materials, low keV imaging can be used to enhance the absorption of high Z material like iodine ($Z = 53$). This can be of particular interest to enhance the iodine uptake for patients with renal dysfunction where the total injected volume of iodinated contrast medium is very limited (Fig. 2.14). Compton scattering on the other hand is dominant at higher keVs and does not exhibit a strong relationship with Z. High keV imaging will then be of particular interest to minimize the absorption of high Z materials and minimize all types of associated artifacts (metal artifacts, calcium, or stent blooming).

References

1. Sun Z. Coronary CT angiography with prospective ECG-triggering: an effective alternative to invasive coronary angiography. Cardiovasc Diagn Ther. 2012;2(1):28–37. https://doi.org/10.3978/j.issn.2223-3652.2012.02.04.
2. Mehta D, Thomson R, Morton T, Dhanantwari A, Shefer E. Iterative model reconstruction: simultaneously lowered computed tomography radiation dose and improved image quality. Med Phys Int. 2013;1:147–55.
3. Isola A, Ziegler A, Köhler T, Niessen W, Grass M. Motion-compensated iterative cone-beam CT image reconstruction with adapted blobs as basis functions. Phys Med Biol. 2008;53:6777–97.
4. Isola A, Grass M, Niessen W. Fully automatic nonrigid registration-based local motion estimation for motion-corrected iterative cardiac CT reconstruction. Med Phys. 2010;37(3):1093–109.
5. Isola A, Ziegler A, Schäfer D, Köhler T, Niessen W, Grass M. Motion compensated iterative reconstruction of a region of interest in cardiac cone-beam CT. Comput Med Imaging Graph. 2010;34:149–59.
6. Garcia MJ, Lessick J, Hoffmann MH. Accuracy of 16-row multidetector computed tomography for the assessment of coronary artery stenosis. JAMA. 2006;296:403–11.
7. Budoff MJ, Dowe D, Jollis JG, Gitter M, Sutherland J, Halamert E, et al. Diagnostic performance of 64-multidetector row coronary computed tomographic angiography for evaluation of coronary artery stenosis in individuals without known coronary artery disease: results from the prospective multicenter ACCURACY (Assessment by Coronary Computed Tomographic Angiography of Individuals Undergoing Invasive Coronary Angiography) trial. J Am Coll Cardiol. 2008;52(21):1724–32.
8. Miller JM, Rochitte CE, Dewey M, Arbab-Zadeh A, Niinuma H, Gottlieb I, et al. Diagnostic performance of coronary angiography by 64-row CT. N Engl J Med. 2008;359(22):2324–36.
9. Meijboom WB, Van Mieghem CA, van Pelt N, Weustink A, Pugliese F, Mollet NR, et al. Comprehensive assessment of coronary artery stenoses: computed tomography coronary angiography versus conventional coronary angiography and correlation with fractional flow reserve in patients with stable angina. J Am Coll Cardiol. 2008;52(8):636–43.
10. Kak A, Slaney M. Principles of computerized tomographic imaging. New York: IEEE; 1988.
11. Kalender WA, Seissler W, Klotz E, Vock P. Spiral volumetric CT with single breath-hold technique, continuous transport and continuous scanner rotation. Radiology. 1990;176:181–3.
12. Crawford CR, King KF. Computed tomography scanning with simultaneous patient translation. Med Phys. 1990;17:967–82.
13. Ohnesorge B, Flohr T, Becker C, Kopp AF, Schoepf UJ, Baum U, et al. Cardiac imaging by means of electrocardiographically gated multi-section spiral CT: initial experience. Radiology. 2001;217:564–71.
14. Feldkamp L, Davis L, Kress J. Practical cone-beam algorithm. J Opt Soc Am A. 1984;1(6):612–9.
15. Grass M, Köhler T, Proksa R. 3D cone-beam CT reconstruction for circular trajectories. Phys Med Biol. 2000;45:329–47.
16. Proksa R, Koehler T, Grass M, Timmer J. The n-PI method for helical cone beam CT. IEEE Trans Med Imaging. 2001;19:848–63.
17. Koehler T, Bontus C, Brown K, Heuscher D, Grass M, Shechter G, et al. Evaluation of helical cone beam CT reconstruction algorithms. IEEE Nucl Sci Symp Conf Rec. 2002;2:1217–20.
18. Grass M, Manzke R, Nielsen T, Koken P, Proksa R, Natanzon M, et al. Helical cardiac cone beam reconstruction using retrospective ECG gating. Phys Med Biol. 2003;48:3069–84.
19. Shechter G, Naveh G, Altman A, Proksa R, Grass M. Cardiac image reconstruction on a 16-slice CT scanner using a retrospectively ECG-gated, multicycle 3D back projection algorithm. Proc SPIE Med Imaging. 2003;5032:1820–8.
20. Muenzel D, Noël PB, Dorn F, Dobritz M, Rummeny EJ, Huber A. Coronary CT angiography in step-and-shoot technique with 256-slice CT: impact of the field of view on image quality, craniocaudal coverage, and radiation exposure. Eur J Radiol. 2012;81(7):1562–8.
21. Vlassenbroek A. The use of isotropic imaging and computed tomography reconstructions. In: Coche EE, Ghaye B, de Mey J, Duyck P, editors. Comparative interpretation of CT and standard radiography of the chest, Medical radiology. Berlin/Heidelberg: Springer; 2011a. https://doi.org/10.1007/978-3-540-79942-9_3.
22. Flohr TG, McCollough CH, Bruder H, Petersilka M, Gruber K, Süss C, et al. First performance evaluation of a dual-source CT (DSCT) system. Eur Radiol. 2006;16:256–68.
23. Achenbach S, Ropers D, Kuettner A, Flohr T, Ohnesorge B, Bruder H, et al. Contrast-enhanced coronary artery visualization by dual-source computed tomography—initial experience. Eur J Radiol. 2006;57:331–5.
24. McCollough CH, Schmidt B, Yu L, Primak A, Ulzheimer S, Bruder H, et al. Measurement of temporal resolution in dual source CT. Med Phys. 2008;35(2).
25. Potel MJ, Rubin JM, MacKay SA, Aisen AM, Al-Sadir J, Sayre RE. Methods for evaluating cardiac wall motion in three dimensions using bifurcation points of the coronary arterial tree. Investig Radiol. 1983;18:47–57.
26. Wang Y, Vidan E, Bergman GW. Cardiac motion of coronary arteries: variability in the rest period and implications for coronary MR angiography. Radiology. 1999;213:751–8.
27. Achenbach S, Ropers D, Holle J, Muschiol G, Daniel WG, Moshage W. In-plane coronary arterial motion velocity: measurement with electron-beam CT. Radiology. 2000;216:457–63.
28. Vembar M, Garcia MJ, Heuscher DJ, Haberl R, Matthews D, Boehme GE, et al. A dynamic approach

to identifying desired physiological phases for cardiac imaging using multislice spiral CT. Med Phys. 2003;30:1683–93.
29. Vembar M, Walker MJ, Johnson PC. Cardiac imaging using multislice computed tomography scanners: technical considerations. Coron Artery Dis. 2006;17:115–23.
30. Gurudevan SV. Postprocessing and reconstruction techniques for the coronary arteries. In: Cardiac CT imaging: diagnosis of cardiovascular disease. London: Springer; 2010. https://doi.org/10.1007/978-1-84882-650-2.
31. Chandra S, Heuscher DJ, Vembar M, Shreter U, Garcia M. Algorithm for acquiring/reconstructing any phase of the heart cycle in multi-slice cardiac CT. First Annual Cardiac CT Conference; 2000 Sept; Heidelberg.
32. Heuscher DJ, Chandra S. Multi-phase cardiac imager. United States Patent 6,510,337. 2003.
33. Manzke R, Köhler T, Nielsen T, Hawkes D, Grass M. Automatic phase determination for retrospectively gated cardiac CT. Med Phys. 2004a;31(12):3345–62.
34. Hoffmann MH, Lessick J, Manzke R, Schmid FT, Gershin E, Boll DT, et al. Automatic determination of minimal cardiac motion phases for computed tomography imaging: initial experience. Eur Radiol. 2006;16:365–73.
35. Stanford W, Rumberger J. Ultrafast computed tomography in cardiac imaging: principles and practice. New York: Futura; 1992.
36. Halpern EJ. Technique, protocols, instrumentation, and radiation dose. In: Clinical cardiac CT, anatomy and function. 2nd ed. Stuttgart, Germany: Thieme Medical Publishers; 2011.
37. Dewey M, Laule M, Krug L, Schnapauff D, Rogalla P, Rutsch W, et al. Multisegment and halfscan reconstruction of 16-slice computed tomography for detection of coronary artery stenosis. Investig Radiol. 2004;39:223–9.
38. Manzke R, Grass M, Nielsen T, Shechter G, Hawkes D. Adaptive temporal resolution optimization in helical cardiac cone beam CT reconstruction. Med Phys. 2003;30:3072–80.
39. Hoffmann MH, Heshui S, Manzke R, Schmid FT, De Vries L, Grass M, et al. Noninvasive coronary angiography with 16-detector row CT: effect of heart rate. Radiology. 2005;234:86–97.
40. van Stevendaal U, Koken P, Begemann PG, Koester R, Adam G, Grass M. ECG gated continuous circular cone-beam multi-cycle reconstruction for in-stent coronary artery imaging: a phantom study. Proc SPIE. 2006;6142:61420L. https://doi.org/10.1117/12.652011.
41. Klass O, Jeltsch M, Feuerlein S, Brunner H, Nagel H-D, Walker MJ, et al. Prospectively gated axial CT coronary angiography: preliminary experiences with a novel low-dose technique. Eur Radiol. 2009;19(4):829–36. https://doi.org/10.1007/s00330-008-1222-4. Epub 2008 Nov 15.
42. Whiting BR, Massoumzadeh P, Earl OA, O'Sullivan JA, Snyder DL, Williamson JF. Properties of preprocessed sinogram data in X-ray computed tomography. Med Phys. 2006;33(9):3290–303.
43. Brown K, Zabic S, Koehler T. Acceleration of ML iterative algorithms for CT by the use of fast start images. Proc. SPIE. 2012;8313:831339. https://doi.org/10.1117/12.911412.
44. Oda S, Weismann G, Vembar M, Weigold WG. Iterative model reconstruction: improved image quality of low-tube-voltage prospective ECG-gated coronary CT angiographyimages at 256-slice CT. Eur J Radiol. 2014. https://doi.org/10.1016/j.ejrad.2014.04.027.
45. Higgins WE, Chung N, Ritman EL. Extraction of left-ventricular chamber from 3-D CT images of the heart. IEEE Trans. Med. Imaging. 1990;9(4):384–94.
46. Redwood AB, Camp JJ, Robb RA. Semiautomatic segmentation of the heart from CT images based on intensity and morphological features. Proc SPIE Med Imaging. 2005;5747:1713–9.
47. Ecabert O, Peters J, Schramm H, Lorenz C, von Berg J, Walker M, et al. Automatic model-based segmentation of the heart in CT images. IEEE Trans Med Imaging. 2008;27(9):1189–201.
48. Ecabert O, Peters J, Walker M, Ivanc T, Lorenz C, von Berg J, et al. Segmentation of the heart and great vessels in CT images using a model-based adaptation framework. Med Image Anal. 2011;15:863–76.
49. Rhode KS, Sermesant M, Brogan D, Hegde S, Hipwell J, Lambiase P, et al. A system for real-time XMR guided cardiovascular intervention. IEEE Trans Med Imaging. 2005;24:1428–40.
50. Knecht S, Skali H, O'Neill MD, Wright M, Matsuo S, Chaudhry GM, et al. Computed tomography-fluoroscopy overlay evaluation during catheter ablation of left atrial arrhythmia. Europace. 2008;10:931–8.
51. Gutiérrez LF, de Silva R, Ozturk C, Sonmez M, Stine AM, Raval AN, et al. Technology preview: X-ray fused with magnetic resonance during invasive cardiovascular procedures. Catheter Cardiovasc Interv. 2007;70:773–82.
52. Lehmann H, Kneser R, Neizel M, Peters J, Ecabert O, Kühl H, et al. Integrating viability information into a cardiac model for interventional guidance. In: Functional imaging and modeling of the heart, FIMH 2009. LNCS, vol. 5528. Berlin/Heidelberg: Springer; 2009. p. 312–20.
53. Hachamovitch R, Berman DS, Shaw LJ, Kiat H, Cohen I, Cabico JA, et al. Incremental prognostic value of myocardial perfusion single photon emission computed tomography for the prediction of cardiac death: differential stratification for risk of cardiac death and myocardial infarction. Circulation. 1998;97(6):535–43.
54. Gerber BL, Belge B, Legros GJ, Lim P, Poncelet A, Pasquet A, et al. Characterization of acute and chronic myocardial infarcts by multidetector computed tomography: comparison with contrast-enhanced magnetic resonance. Circulation. 2006;113(6):823–33.
55. Gerber BL, Rochitte CE, Melin JA, McVeigh ER, Bluemke DA, Wu KC, et al. Microvascular obstruction and left ventricular remodeling early after acute myocardial infarction. Circulation. 2000;101:2734–41.

56. Gerber BL, Garot J, Bluemke DA, Wu KC, Lima JA. Accuracy of contrast-enhanced magnetic resonance imaging in predicting improvement of regional myocardial function in patients after acute myocardial infarction. Circulation. 2002;106:1083–9.
57. Blankstein R, Okada DR, Rocha-Filho JA, Rybicki FJ, Brady TJ, Cury RC. Cardiac myocardial perfusion imaging using dual-source computed tomography. Int J Cardiovasc Imaging. 2009. https://doi.org/10.1007/s10554-009-9438-1.
58. Blankstein R, Shturman LD, Rogers IS, Rocha-Filho JA, Okada DR, Sarwar A, et al. Adenosine-induced stress myocardial perfusion imaging using dual-source cardiac computed tomography. J Am Coll Cardiol. 2009;54(12):1072–84. https://doi.org/10.1016/j.jacc.2009.06.014.
59. George RT, Arbab-Zadeh A, Miller JM, Kitagawa K, Chang HJ, Bluemke DA, et al. Adenosine stress 64- and 256-row detector computed tomography angiography and perfusion imaging. A pilot study evaluating the transmural extent of perfusion abnormalities to predict atherosclerosis causing myocardial ischemia. Circ Cardiovasc Imaging. 2009;2:174–82. https://doi.org/10.1161/circimaging.108.813766.
60. Lessick J, Dragu R, Mutlak D, Rispler S, Beyar R, Litmanovich D, et al. Is functional improvement after myocardial infarction predicted with myocardial enhancement patterns at multidetector CT? Radiology. 2007;244(3):736–44. https://doi.org/10.1148/radiol.2443061397. Epub 2007 Aug 9.
61. Mahnken AH, Klotz E, Pietsch H, Schmidt B, Allmendinger T, Haberland U, et al. Quantitative whole heart stress perfusion CT imaging as noninvasive assessment of hemodynamics in coronary artery stenosis: preliminary animal experience. Investig Radiol. 2010;45(6):298–305. https://doi.org/10.1097/RLI.0b013e3181dfa3cf.
62. Bamberg F, Klotz E, Flohr T, Becker A, Becker CR, Schmidt B, et al. Dynamic myocardial stress perfusion imaging using fast dual-source CT with alternating table positions: initial experience. Eur Radiol. 2010;20(5):1168–73. https://doi.org/10.1007/s00330-010-1715-9. Epub 2010 Mar 24.
63. Bamberg F, Becker A, Schwarz F, Marcus RP, Greif M, von Ziegler F, et al. Detection of hemodynamically significant coronary artery stenosis: incremental diagnostic value of dynamic CT-based myocardial perfusion imaging. Radiology. 2011;260(3):689–98. https://doi.org/10.1148/radiol.11110638.
64. Gramer BM, Muenzel D, Leber V, von Thaden AK, Feussner H, Schneider A, et al. Impact of iterative reconstruction on CNR and SNR in dynamic myocardial perfusion imaging in an animal model. Eur Radiol. 2012;22(12):2654–61. https://doi.org/10.1007/s00330-012-2525-z. Epub 2012 Jul 3.
65. Kurata A, Kawaguchi N, Kido T, Inoue K, Suzuki J, Ogimoto A, et al. Qualitative and quantitative assessment of adenosine triphosphate stress whole-heart dynamic myocardial perfusion imaging using 256-slice computed tomography. PLoS One. 2013;8(12):e83950. https://doi.org/10.1371/journal.pone.0083950. eCollection 2013.
66. Huber AM, Leber V, Gramer BM, Muenzel D, Leber A, Rieber J, et al. Myocardium: dynamic versus single-shot CT perfusion imaging. Radiology. 2013;269(2):378–86. https://doi.org/10.1148/radiol.13121441. Epub 2013 Jun 20.
67. Muenzel D, Kabus S, Gramer B, Leber V, Vembar M, Schmitt H, et al. Dynamic CT perfusion imaging of the myocardium: a technical note on improvement of image quality. PLoS One. 2013;8(10):e75263. https://doi.org/10.1371/journal.pone.0075263. eCollection 2013.
68. Muenzel D, Noël PB, Gramer BM, Leber V, Schneider A, Leber A, et al. Dynamic CT perfusion imaging of the myocardium using a wide-detector scanner: a semi-quantitative analysis in an animal model. Clin Imaging. 2014;38(5):675–80. https://doi.org/10.1016/j.clinimag.2014.05.011. Epub 2014 Jun 2.
69. Isola AA, Schmitt H, van Stevendaal U, Begemann PG, Coulon P, Boussel L, et al. Image registration and analysis for quantitative myocardial perfusion: application to dynamic circular cardiac CT. Phys Med Biol. 2011;56(18):5925–47. https://doi.org/10.1088/0031-9155/56/18/010. Epub 2011 Aug 22.
70. Eck B, Fahmi R, Wen G, Fuqua C, Vembar M, Dhanantwari A, et al. Low dose dynamic myocardial CT perfusion using advanced iterative reconstruction. Proc. SPIE. 2014;9417:94170Z. https://doi.org/10.1117/12.2081418.
71. Fahmi R, Eck BL, Vembar M, Bezerra HG, Wilson DL. Dose reduction assessment in dynamic CT myocardial perfusion imaging in a porcine balloon-induced-ischemia model. Proc. SPIE. 2014;9033:903305. https://doi.org/10.1117/12.2043748.
72. Koo BK, Erglis A, Doh JH, Daniels DV, Jegere S, Kim HS, et al. Diagnosis of ischemia-causing coronary stenoses by noninvasive fractional flow reserve computed from coronary computed tomographic angiograms. Results from the prospective multicenter DISCOVER-FLOW (Diagnosis of Ischemia-Causing Stenoses Obtained Via Noninvasive Fractional Flow Reserve) study. J Am Coll Cardiol. 2011;58(19):1989–97. https://doi.org/10.1016/j.jacc.2011.06.066.
73. Min JK, Leipsic J, Pencina MJ, Berman DS, Koo BK, van Mieghem C, et al. Diagnostic accuracy of fractional flow reserve from anatomic CT angiography. JAMA. 2012;308(12):1237–45.
74. Nørgaard BL, Leipsic J, Gaur S, Seneviratne S, Ko BS, Ito H, et al. NXT Trial Study Group. Diagnostic performance of noninvasive fractional flow reserve derived from coronary computed tomography angiography in suspected coronary artery disease: the NXT trial (Analysis of Coronary Blood Flow Using CT Angiography: Next Steps). J Am Coll Cardiol. 2014;63(12):1145–55. https://doi.org/10.1016/j.jacc.2013.11.043. Epub 2014 Jan 30.
75. Manzke R, Grass M, Hawkes D. Artifact analysis and reconstruction improvement in helical cardiac cone beam CT. IEEE Trans. Med. Imaging. 2004b;23(9):1150–64.

76. von Berg J, Barschdorf H, Blaffert T, Kabus S, Lorenz C. Surface based cardiac and respiratory motion extraction for pulmonary structures from multi-phase CT. Proc SPIE Med Imaging Conf. 2007;6511:65110Y-1–65110Y-11.
77. Peters J, Ecabert O, Schmitt H, Grass M, Weese J. Local cardiac wall motion estimation from retrospectively gated CT images. In: Ayache N, Delingette H, Sermesant M, editors. FIMH 2009, LNCS 5528; 2009; pp. 191–200.
78. Hansis E, Schomberg H, Erhard K, Dössel O, Grass M. Four-dimensional cardiac reconstruction from rotational x-ray sequences: first results for 4D coronary angiography. In: Samei E, Hsieh J, editors. Medical imaging 2009: physics of medical imaging, 72580B; 2009.
79. Rohkohl C, Lauritsch G, Biller L, Prümmer M, Boese J, Hornegger J. Interventional 4D motion estimation and reconstruction of cardiac vasculature without motion periodicity assumption. Med Image Anal. 2010;14:687–94.
80. Forthmann P, van Stevendaal U, Grass M, Köhler T. Vector field interpolation for cardiac motion compensated reconstruction. Proceeding of the IEEE NSS-MIC Conference; 2008.
81. van Stevendaal U, von Berg J, Lorenz M, Grass M. A motion-compensated scheme for helical cone-beam reconstruction in cardiac CT angiography. Med Phys. 2008;35(7):3239–51.
82. Schäfer D, Borgert J, Rasche V, Grass M. Motion-compensated and gated cone beam filtered back-projection for 3-D rotational X-ray angiography. IEEE Trans Med Imaging. 2006;25(7):898–906.
83. Schirra C, Bontus C, van Stevendaal U, Dössel O, Grass M. Improvement of cardiac CT reconstruction using local motion vector fields. Comput Med Imaging Graph. 2009;33:122–30.
84. Fornaro J, Leschka S, Hibbeln D, Butler A, Anderson N, Pache G, et al. Dual- and multi-energy CT: approach to functional imaging. Insights Imaging. 2011;2:149–59.
85. Vlassenbroek A, Dual Layer CT. Dual energy CT in clinical practice, Medical radiology. Berlin/Heidelberg: Springer; 2011b. https://doi.org/10.1007/978-3-642-01740-7.
86. Maass N, Baer M and Kachelriess M. Image-based dual energy CT using optimized precorrection functions: a practical new approach of material decomposition in image domain. Med Phys. 2009;36(8).
87. Fahmi R, Eck BL, Fares A, Levi J, Wu H, Vembar M, et al. Dynamic myocardial perfusion in a porcine balloon-induced ischemia model using a prototype spectral detector CT. Proc. SPIE. 2015;9417:94170Y-8.
88. Engel KJ, Herrmann C, Zeitler G. X-ray scattering in single and dual-source CT. Med Phys. 2008;35(1):318–32.
89. Alvarez RE, Macovski A. Energy-selective reconstructions in X-ray computerized tomography. Phys Med Biol. 1976;21(5):733–44.
90. Goodsitt MM, Christodoulou EG, Larson SC. Accuracies of the synthesized monochromatic CT numbers and effective atomic numbers obtained with a rapid kVp switching dual energy CT scanner. Med Phys. 2011;38:2222–32.
91. Yu L, Leng S, McCollough CH. Dual energy CT-based monochromatic imaging. AJR Am J Roentgenol. 2012;199(5 Suppl):S9–S15.